To the Graduate Council:

I am submitting herewith a thesis written by Jefferson K. Jordan entitled "Computational Investigation of Mutual Interference Effects on the Influence Function Method of Store Load Prediction." I have examined the final copy of this thesis for form and content and recommend that it be accepted in partial fulfillment of the requirements for the degree of Master of Science, with a major in Aerospace Engineering.

Dr. E.M. Kraft, Major Professor

We have read this thesis
and recommend its acceptance:

Accepted for the Council:

Associate Vice Chancellor
and Dean of the Graduate School

STATEMENT OF PERMISSION TO USE

In presenting this thesis in partial fulfillment of the requirements for a Master's degree at The University of Tennessee, Knoxville, I agree that the Library shall make it available to borrowers under rules of the Library. Brief quotations from this thesis are allowable without special permission, provided that accurate acknowledgment of the source is made.

Permission for extensive quotation from or reproduction of this thesis may be granted by my major professor, or in his absence, by the Head of Interlibrary Services when, in the opinion of either, the proposed use of the material is for scholarly purposes. Any copying or use of the material in this thesis for financial gain shall not be allowed without my written permission.

Signature J. Keith Jordan

Date 11-22-91

Computational Investigation of Mutual Interference Effects on the Influence Function Method of Store Load Prediction

A Thesis
Presented for the
Master of Science
Degree
The University of Tennessee, Knoxville

Jefferson K. Jordan
December, 1991

DEDICATION

To my two most important reasons for obtaining a Master's Degree— my wife, Margaret, and my son, Scott.

ACKNOWLEDGMENTS

I would like to thank the employees of Calspan Corporation, AEDC Operations, who assisted in this study and the preparation of this thesis. In particular: Dr. J.A. Benek, W.E. Dietz, T.L. Donegan, Dr. J.C. Erickson , Dr. J.H. Fox, E.R. Heim, Dr. J.L. Jacocks, Dr. S.L. Keeling, K.S. Keen, Dr. E.M. Kraft, Dr. R.H. Nichols, and N.E. Suhs. Their tutelage was invaluable and their patience greatly appreciated. I would also like to thank Dr. K.C. Reddy, Dr. A.D. Vakili, and Dr. H.J. White for their assistance in editing this thesis.

ABSTRACT

Steady-state numerical solutions of the Euler equations for the flow field about a wing/pylon/finned store configuration at a Mach number of 0.95 have been obtained for several store locations and attitudes. The objectives of the study were to gain insight into requirements for future computational trajectory prediction methods, to compare computational loads and pressures to test data, and to investigate a mutual interference correction implemented in a semi-empirical trajectory program. To meet these objectives, CFD solutions were obtained placing the store at the carriage position, at 0.25, 0.50, 1.0, and 4.0 store body diameters below the carriage position, and at a position determined by the wind tunnel trajectory simulation test. Load predictions were also obtained from the trajectory program for these positions. The CFD pressure distributions for the store at the carriage and trajectory positions agreed well with the measured test data, and the CFD loads on the store in these two cases agreed fairly well with the test loads. Conversely, the loads from the basic semi-empirical trajectory prediction program were in poor agreement with the measured loads and CFD loads in all cases. However, when properly applied, the mutual interference loads corrections in the trajectory prediction program provide a reasonable approximation to the CFD loads. Over the course of this investigation, it was found that grid density, geometric accuracy, and viscosity requirements for future CFD trajectory predictions are extremely dependent on the physical properties of the store of interest and the method of release.

Contents

1 INTRODUCTION 1

1.1 Background 1

1.2 Objective of Study and Approach 2

2 MODELS AND TEST DESCRIPTION 6

3 OFF-LINE TRAJECTORY PREDICTION 13

3.1 The Influence Function Method 14

3.2 Carriage Load Corrections 16

4 DOMAIN DECOMPOSITION PHILOSOPHY 17

4.1 Grid Generation 18

4.1.1 Subgrids 19

4.2 Inter-grid Communication 29

4.3 Solving the Euler Equations 29

4.3.1 General 29

4.3.2 Boundary Conditions 30

5 RESULTS AND DISCUSSION 32

6 CONCLUSIONS 58

BIBLIOGRAPHY 60

VITA 63

List of Figures

1.1 Test article 3

2.1 Wing geometry viewed from below 7

2.2 Pylon geometry 8

2.3 Store geometry 9

2.4 Store pressure tap locations 10

3.1 The IFM representation of a store 15

4.1 Fin grids 20

4.2 Store/sting grids 21

4.3 Pylon grids 22

4.4 Wing grids 24

4.5 Aerodynamic Wind Tunnel (4T) grid with wing/pylon/store superimposed 25

4.6 Store communication grid with store/sting superimposed 26

4.7 Wing communication grid with wing/pylon/store superimposed 28

5.1 Pressure coefficient distribution at the carriage position 33

5.2 Pressure coefficient distribution at Δz= -0.25 DIA 36

5.3 Pressure coefficient distribution at Δz= -0.50 DIA 38

5.4 Pressure coefficient distribution at Δz= -1.00 DIA 40

5.5 Pressure coefficient distribution at Δz= -4.00 DIA 42

5.6 Comparison of pressure coefficient distributions 44

5.7 IFM influence coefficients and associated flow angles 47

5.8 Pressure coefficient contours along store symmetry plane 48

5.9 Wing lower surface pressure coefficient contours 50

5.10 Store in trajectory position 51

5.11 Pressure coefficient distribution at the trajectory position 52

5.12 IFM carriage load corrections 56

LIST OF SYMBOLS

$ANCN_i$	Influence coefficient used by the Influence Function Method to calculate normal and side forces.
$BNCLM_i$	Influence coefficients used by the Influence Function Method to calculate yawing and pitching moment coefficients.
c	Store model fin local chord.
c.g.	Store center of gravity located 2.79 inches (model scale) from the store nose.
C_l	Rolling moment coefficient of the store model, (rolling moment)/(Q*S*DIA)
C_m	Pitching moment coefficient of the store model taken about the c.g., (pitching moment)/(Q*S*DIA).
C_N	Normal force coefficient of the store model, (normal force)/(Q*S).
C_n	Yawing moment coefficient of the store model taken about the c.g., (yawing moment)/(Q*S*DIA).
c_p	Pressure coefficient, $(P_{local} - P_{FS})/Q$.
C_Y	Side force coefficient of the store model, (side force)/(Q*S).
DIA	Store model diameter, 1.0 in. (model scale)
FS	Free stream
L	Store model length, 5.941 in. (model scale)
M	Free stream Mach number.
Q	Free stream dynamic pressure, 424.9 psf.
S	Store model cross-sectional area, 0.7854 in^2. (model scale)
α_{xz}	Upwash angle.
α_{xy}	Sidewash angle.

$\Delta x, \Delta y, \Delta z$	Translated x, y, and z distance in store body diameters of the store's c.g. from the carriage position.
ξ, η, ζ	Computational grid curvilinear coordinates.
ϕ	Azimuthal angle location on store.

Subscripts

$(\ )_{car}$	Load coefficient ( ) of the store at the store carriage orientation.
$(\ )_{FS}$	Load coefficient ( ) of the store at a specific orientation in a free-stream flow with no wing.
$(\ )_{IFM}$	Load coefficient ( ) of the store calculated using the IFM.

Chapter 1

INTRODUCTION

1.1 Background

As the speed of attack aircraft has increased, so, too, have the problems associated with store release. At high speeds, strong upwash and sidewash can force a store to extreme pitch and yaw orientations and thereby cause the store to miss the target widely or even strike the parent aircraft. Moreover, unacceptably large release attitudes may result from the severe upwash and sidewash that exist inside the weapons bays that some of the latest generation aircraft utilize. Time consuming and expensive wind tunnel and flight tests are required to determine whether a store will fall away from the aircraft with an acceptable attitude and displacement at many aircraft attitudes, altitudes and Mach numbers. This certification process can cost millions of dollars and take several years to complete. It is apparent, then, why less expensive and faster computational store trajectory prediction methods are being pursued.

In any trajectory prediction process, the accurate prediction of the forces and moments on a moving store in a complex flow field is of paramount importance. However, this force prediction capability is currently beyond the reach of many computational methods. Some semi-empirical computational methods have been used for several years and have been providing very useful information with relatively high accuracy and small expense [1], [2], but they incorporate simplifications and empirical corrections that may not prove to be adequate in supersonic flight

envelopes or with the release from a weapons bay. The capabilities of computational fluid dynamics (CFD) are rapidly being expanded, but currently have not been proven to be able to fully predict trajectory loads on the complex bodies involved at a reasonable cost and with reliable accuracy. It has been shown, however, that CFD has matured to a level which, when coupled with the analytic methods, can aid in the store certification process [3], [4], and perhaps improve the accuracy of the analytic methods.

At the Arnold Engineering Development Center (Arnold AFB, Tennessee), or AEDC, one method of trajectory prediction uses wind tunnel data in conjunction with an off-line computer code employing the Influence Function Method (IFM) [1] to calculate the required forces on the store. There are drawbacks to the IFM, however. Its primary assumption is that the store does not affect the aircraft flow field; that is, no mutual interference is modeled. This assumption has proven to be acceptable away from the aircraft, but mutual interference that occurs between the aircraft and store near the aircraft can be quite substantial. (A quantitative definition of 'near' is currently undetermined.) The trajectory prediction code includes a correction to the forces near the carriage position, but the validity of this correction has not been thoroughly investigated.

1.2 Objective of Study and Approach

The purpose of this study is to (1) gain insight into future requirements for using CFD for trajectory prediction, (2) compare computational pressure and load predictions to test data, and (3) estimate the error involved in the mutual interference correction for the IFM method. Solutions of the Euler equations at M=0.95 were obtained for seven cases. The Euler equations were chosen over the Navier Stokes equations because previous computations seemed to indicate that inviscid solutions would be sufficient and significant savings in time and expense would be realized [3], [4]. The wing/pylon/finned store configuration to be studied is shown in Fig. 1.1. The wing remained at zero angle of attack in all calculations. All but two cases used the same configuration with the store placed in different prescribed positions below the carriage position.

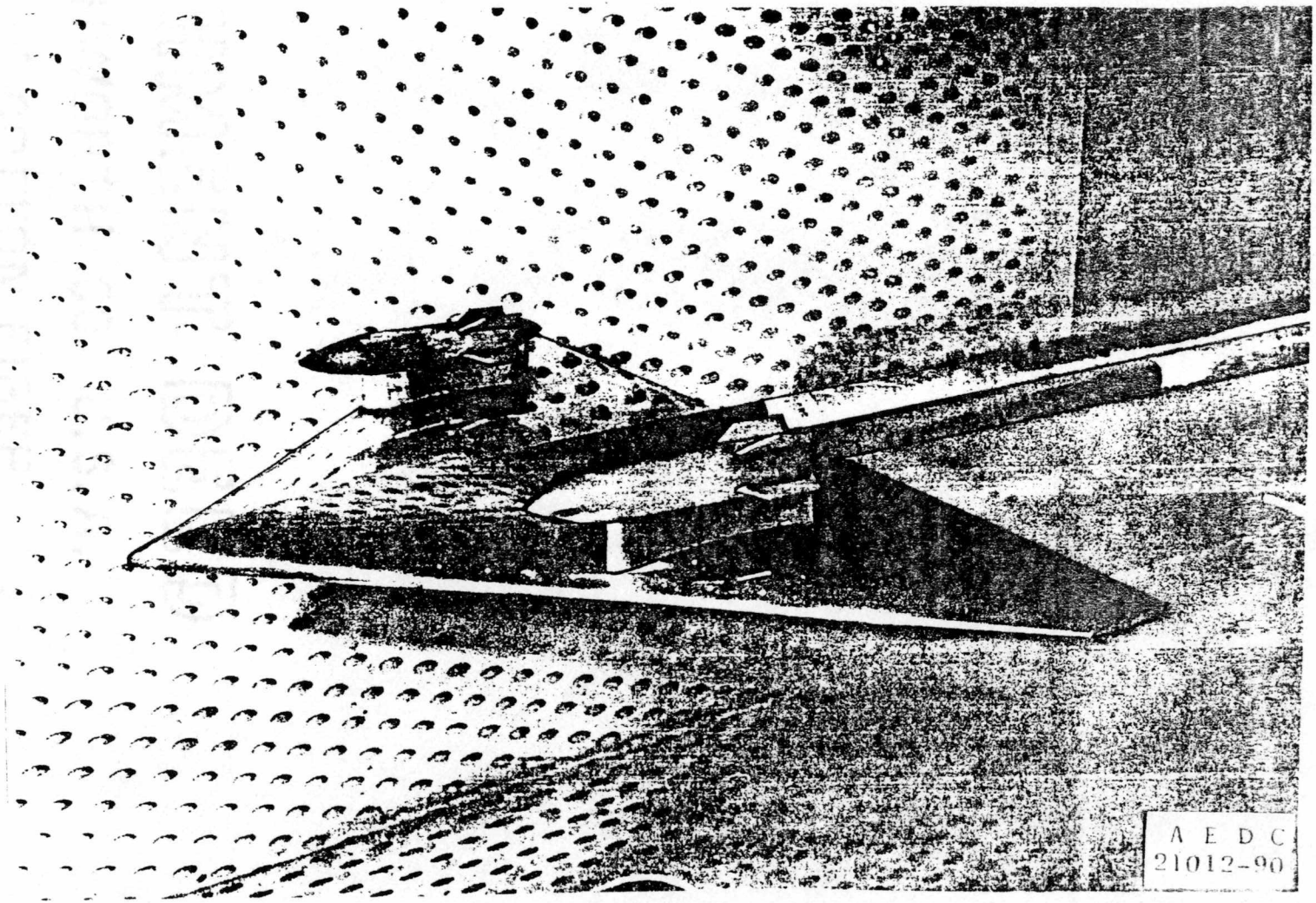

Figure 1.1: Test article

These prescribed positions had no relation to locations through which the free-falling store would pass. The first case located the store below the pylon at zero yaw, pitch and roll relative to the free stream with a 0.07 store diameter gap between the pylon and store to match the carriage position of the wind tunnel test. The next four cases placed the store 0.25, 0.50, 1.0, and 4.0 store diameters directly below the carriage position with zero yaw, pitch and roll relative to the free stream. One case modeled only the wing/pylon in the tunnel and was necessary to determine flow angles required by the IFM to predict loads. This case was necessary because the required data were not obtained in the test. The final calculation oriented the store at an actual trajectory position determined by the wind tunnel test. In each case, calculated loads on the store were determined and compared to the loads predicted by the IFM (which used the CFD predicted flow angles), and at the carriage and trajectory position, both the calculated pressures and forces were compared to test data. For clarity, Table 1.1 lists all cases studied.

Table 1.1: Cases studied

Case	Δ x	Δ y	Δ z	Yaw	Pitch	Roll
1. wing/pylon	-	-	-	-	-	-
2. wing/pylon/store	0.00	0.00	0.00	0.00	0.00	0.00
3. wing/pylon/store	0.00	0.00	-0.25	0.00	0.00	0.00
4. wing/pylon/store	0.00	0.00	-0.50	0.00	0.00	0.00
5. wing/pylon/store	0.00	0.00	-1.00	0.00	0.00	0.00
6. wing/pylon/store	0.00	0.00	-4.00	0.00	0.00	0.00
7. wing/pylon/store	0.50	-0.19	-2.48	-12.37^o	2.76^o	-6.50^o

Chapter 2

MODELS AND TEST DESCRIPTION

The dimensions in all of the following figures are model scale. Even though no corresponding full scale geometry exists, a 5% scale model was assumed in the trajectory test for scaling the loads used by the trajectory prediction program, FLOWTGP [1]. The wing (shown in Fig. 2.1) has a clipped delta wing planform with a NACA 64A010 symmetric airfoil section. The pylon geometry is presented in Fig. 2.2. Figure 2.3 depicts the store model, which has a tangent-ogive forebody and afterbody with four fins. The afterbody is truncated by an attached sting. The fin cross-sections are NACA 0008 airfoils.

On the wing and pylon, 146 orifices at chordwise row locations were used to measure static pressure. Two store models were used, one for force data and the other for pressure data. A single model could not be used because the model interior was not large enough to contain hardware for both pressure and force data. The pressure model was unusually well instrumented with five rows of 28 pressure taps on the body and two chordwise rows on one side of each fin (see Fig. 2.4). Pressure distributions along the length of the store at 10 degree azimuthal intervals and more complete data on the fins were obtained by rolling the store through 90 degree increments and moving the store to the opposite side of the wing symmetry plane. A pylon and fixed store were attached on the side opposite the instrumented store to maintain a vertical plane of symmetry,

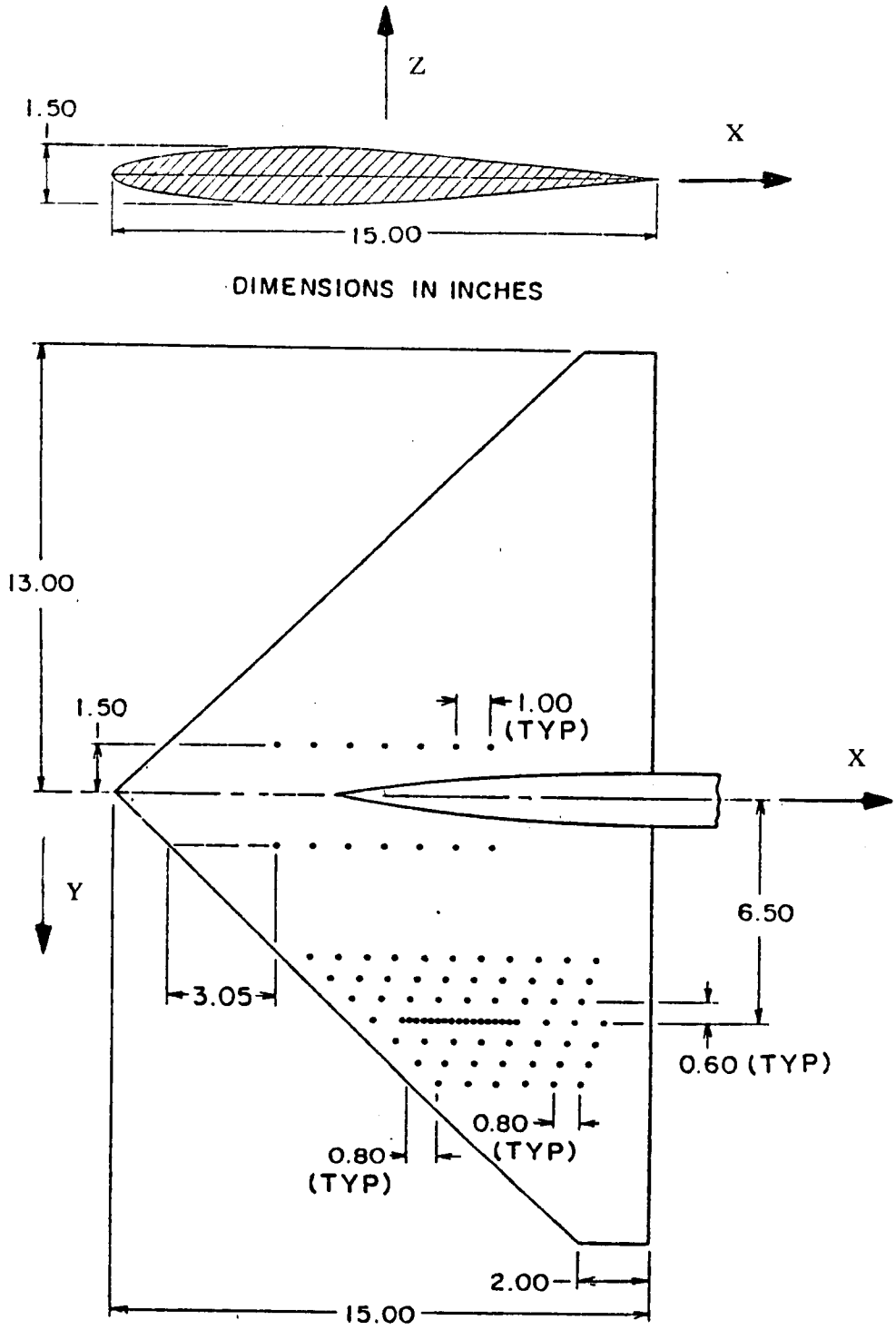

Figure 2.1: Wing geometry viewed from below

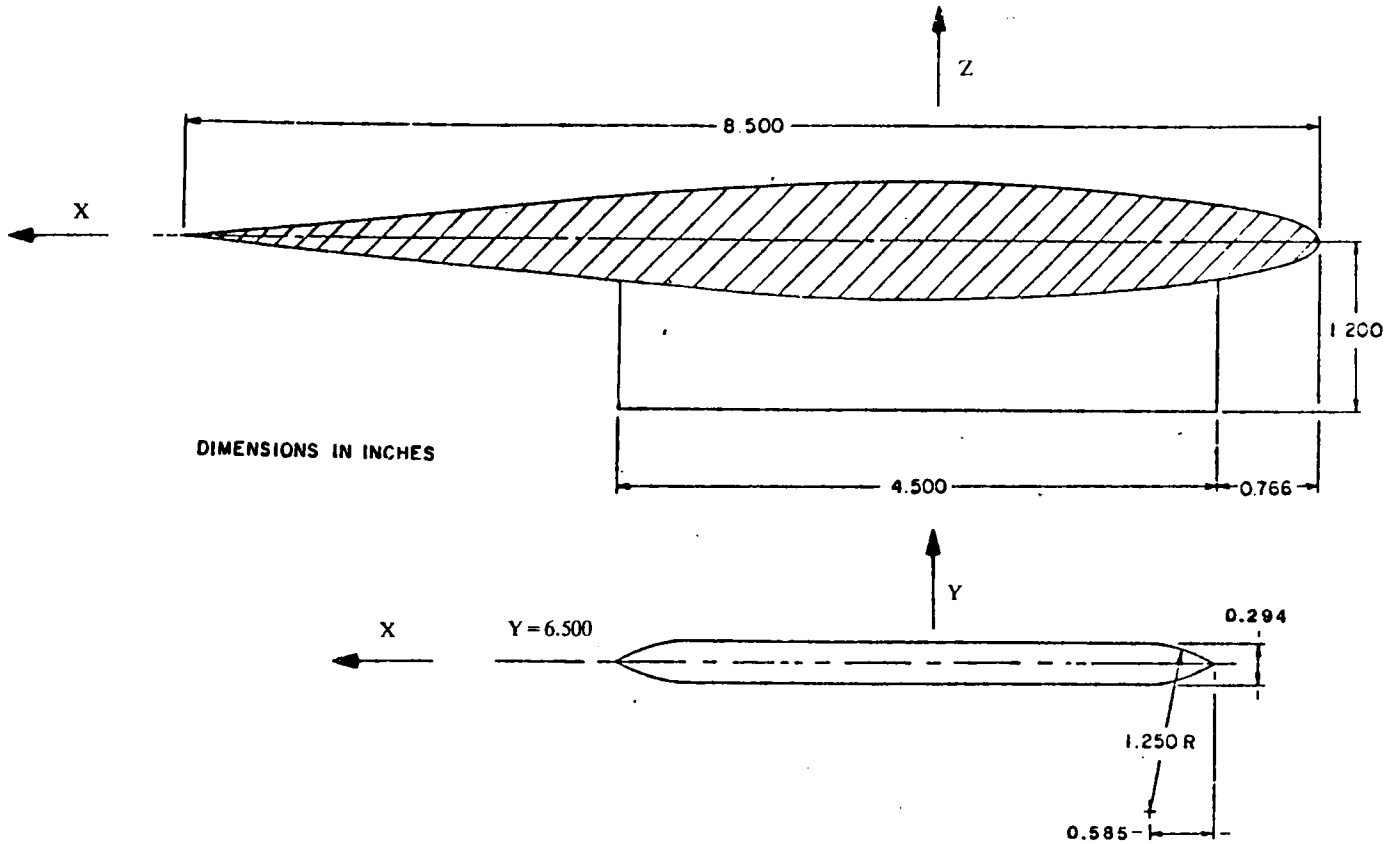

Figure 2.2: Pylon geometry

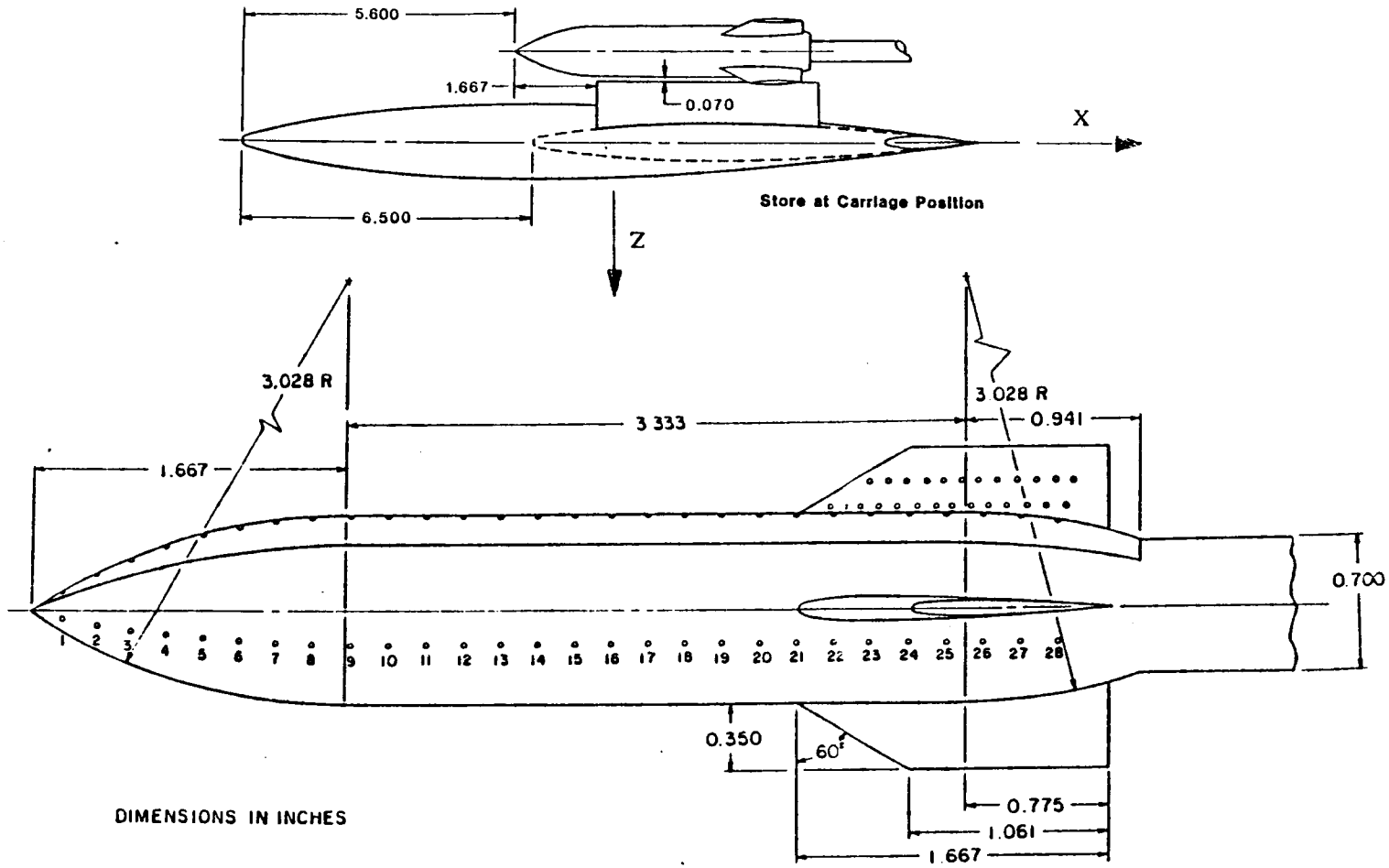

Figure 2.3: Store geometry

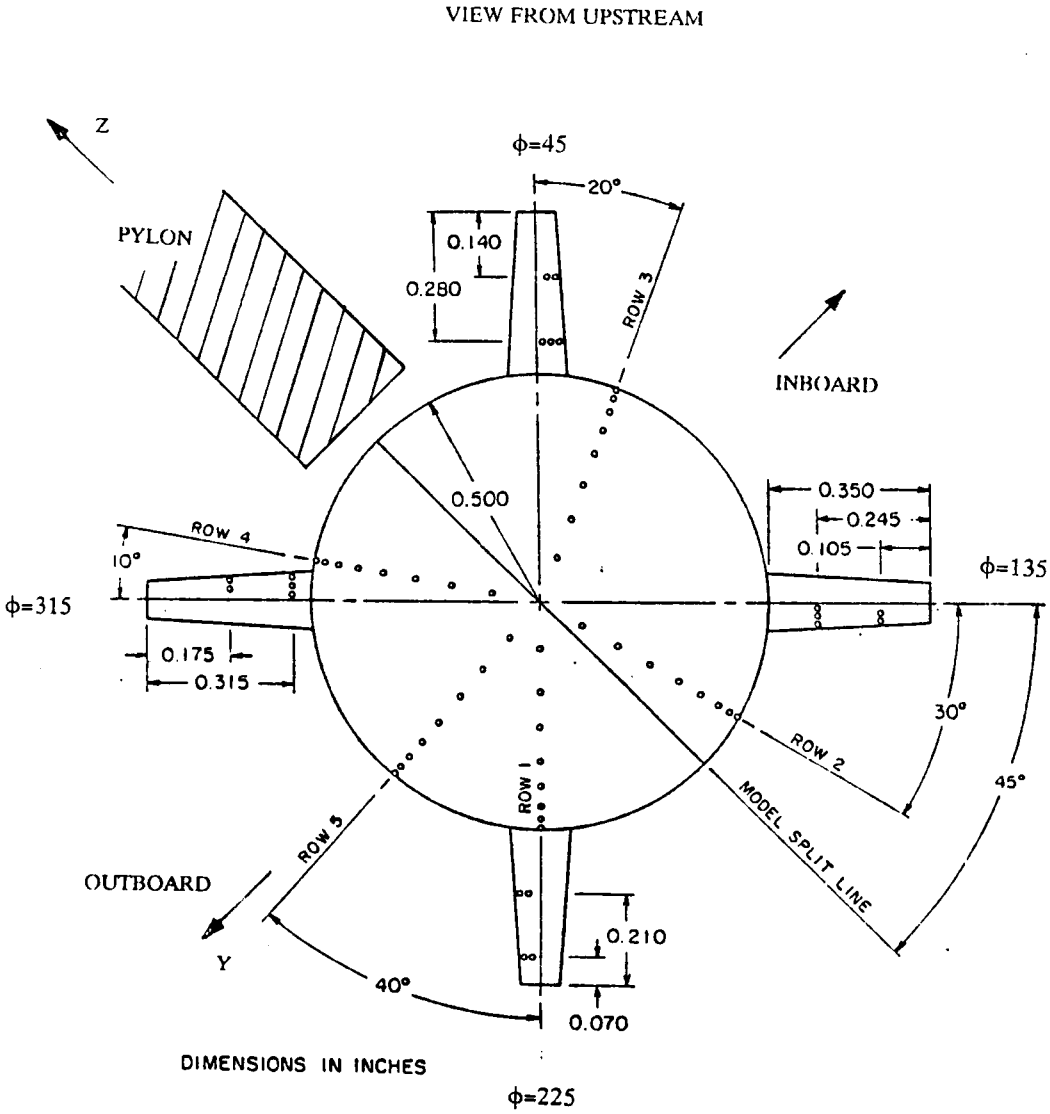

Figure 2.4: Store pressure tap locations

insofar as was possible (see Fig. 1.1).

The tests for this model were sponsored by the AFATL/FXA, Eglin AFB, Florida and were conducted at the AEDC in the Aerodynamic Wind Tunnel (4T) [5]. The Aerodynamic Wind Tunnel (4T) is a continuous flow transonic tunnel with a Mach number capability ranging from 0.1 to 2.0. The test section has a 4 ft. square cross-section and is 12 ft. long with variable porosity walls. The wind tunnel walls were modeled in all the calculations with the wall porosity effects being modeled with boundary conditions (see Section 4.3.2).

Data were acquired using the Captive Trajectory Support (CTS) [6] system. The CTS system uses independently movable stings for the parent craft and store. To predict a trajectory, one of three modes is used, two of which are pertinent to this study. In one mode, the point-prediction mode, balances measure the forces acting on the store at its current location and attitude. The forces are then used to predict the motion of the store over some small time step (typically 2.5 milliseconds) by integrating the six degree-of-freedom equations of motion. The store is then moved to the new location and the process is repeated until the desired distance from the parent craft is reached.

In another mode, the grid mode, flow-field properties, including flow angles, are measured at discrete spacial locations in the region of the expected trajectory. FLOWTGP [1], the off-line trajectory prediction code, then uses the flow angles and the IFM [1] to calculate the forces on the store at a given trajectory point. The equations of motion are then integrated and the store is moved to its new location. This procedure is repeated until the store has moved a prescribed distance from the starting position. One very important advantage of the grid mode is that once the aircraft flow field is adequately mapped out, trajectories of other stores can be predicted without additional tunnel tests.

Data used in this study were obtained at a Mach number of 0.95. Trajectory data were generated in the point-prediction mode for the store force model with the wing at zero angle of attack. Pressure data also were obtained with the store at two discrete trajectory locations that

had been previously determined by the point-prediction mode test (cases 2 and 7).

Chapter 3

OFF-LINE TRAJECTORY PREDICTION

In the FLOWTGP [1] trajectory prediction procedure, the total loads acting on the store are determined by separating the forces and moments in an aircraft flow field into loads on the store in a free-stream flow, and changes in the loads caused by the presence of the aircraft. The IFM [1] is used to predict the loads acting on the store at a trajectory orientation in the aircraft flow field and in the same orientation in a free-stream flow field. A 'delta coefficient' is then calculated by subtracting the IFM predicted free-stream store loads from the IFM predicted aircraft-flow-field store loads. If C represents some load coefficient, then

$$\Delta_1 C = C_{IFM} - C_{IFM_{FS}}$$

Delta coefficients are then added to the loads on the store in a measured free-stream flow at an adjusted orientation to determine the complete loads on the store. The adjusted orientation is the trajectory orientation plus induced angles that would be caused by the translational movement of the free-falling store (tunnel hardware constraints preclude moving the store in real time). Rotational velocity effects are accounted for elsewhere in FLOWTGP. The delta coefficient method is used because force calculations are often incorrect (compared to data) in an absolute sense, but the differences between calculated loads in an aircraft flow field and the corresponding loads

calculated in a free-stream flow field are very close to measured differences.

3.1 The Influence Function Method

A concept that is vital to an understanding of the IFM [1] is that the IFM does not have a strictly aerodynamic derivation; the method is based primarily on mathematical correlations of empirical data. A simple cause/effect relationship is assumed; the loads on the store are the effect of the local upwash and sidewash impinging on the store. The IFM represents the store mathematically as the sum of a number of segments dividing the store along its length (see Fig. 3.1). Each segment is assumed to affect the total loads differently depending on its shape and the angle of the flow impinging on that segment. Force and moment coefficients are represented as the summation of the products of the flow angles at the centroid of each segment and an 'influence coefficient' for that segment. Specifically,

$$
\begin{aligned}
C_N &= \sum_{i=1}^{N} \mathrm{ANCN}_i \cdot \alpha_{xz_i} + C_{N_0}, \\
C_m &= \sum_{i=1}^{N} \mathrm{BNCLM}_i \cdot \alpha_{xz_i} + C_{m_0}, \\
C_Y &= \sum_{i=1}^{N} \mathrm{ANCN}_i \cdot \alpha_{xy_i} + C_{Y_0}, \\
C_n &= \sum_{i=1}^{N} \mathrm{BNCLM}_i \cdot \alpha_{xy_i} + C_{n_0},
\end{aligned}
$$

where ANCN_i and BNCLM_i are the influence coefficients of each segment, α_{xy} and α_{xz} are the upwash and sidewash angles, and the terms with subscript zero are the coefficients when the store is at zero pitch, yaw, and roll. Ideally, these zero pitch/yaw/roll coefficients should be zero for an axisymmetric body with fins that have symmetrical cross-sections and zero incidence with respect to the store centerline. However, inaccuracies in the model (a bent fin, for example) often are present, requiring a correction. The axial force and rolling moment cannot currently be

$$C_N = \sum_{i=1}^{N} \mathrm{ANCN}_i \cdot \alpha_{xz_i} + C_{N_0},$$

$$C_m = \sum_{i=1}^{N} \mathrm{BNCLM}_i \cdot \alpha_{xz_i} + C_{m_0},$$

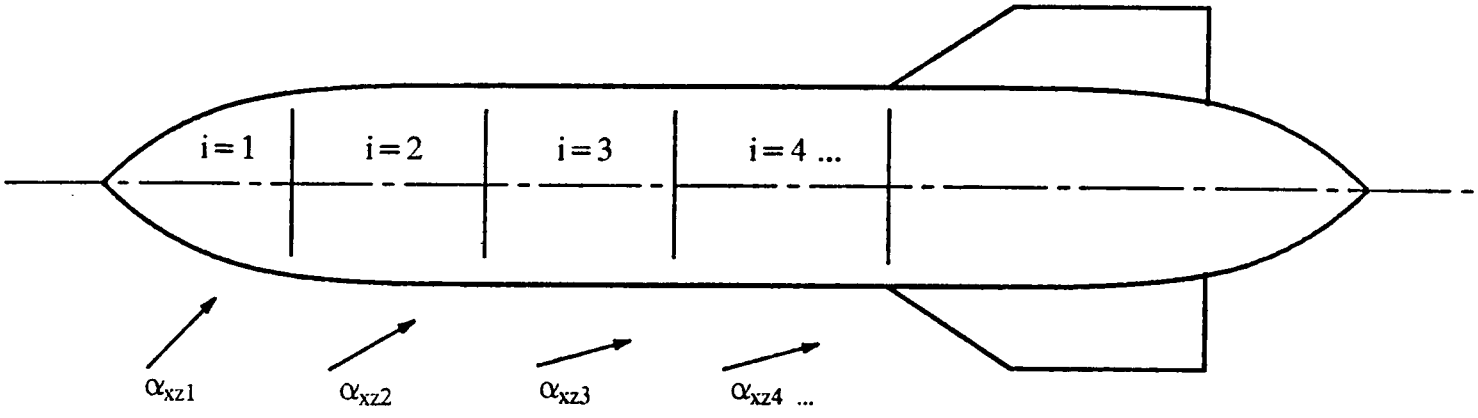

Figure 3.1: The IFM representation of a store

determined by the IFM; axial force and rolling moment are assumed to be empirical functions of the store orientation relative to the free stream.

3.2 Carriage Load Corrections

A correction for the calculated delta coefficients near the carriage position (where the mutual interference is most significant) is included in FLOWTGP. Loads are measured on the store at the carriage position with and without the aircraft model installed in the tunnel. An experimental carriage delta coefficient is then calculated by subtracting the measured free-stream carriage loads from the measured aircraft-flow-field carriage loads.

$$\Delta_{car}C = C_{car} - C_{car_{FS}}$$

A 'double' delta coefficient is obtained by subtracting the IFM predicted delta at carriage from the experimental carriage delta.

$$\Delta\Delta C = \Delta_{car}C - (\Delta_1 C)_{car}$$

This double delta correction is fully applied to $\Delta_1 C$ at carriage and then allowed to decay according to a sine function. This decay function was an assumption introduced by the test engineers and has no rigorous aerodynamic basis. Since the store was restrained to zero pitch and yaw in this study, some of the above terms go to zero so that the equations for the load coefficients become

$$C = C_{IFM} + C_{car} - C_{IFM_{car}} - (C_{car} - C_{IFM_{car}}) \sin\left(\frac{\pi}{2} \cdot \frac{\Delta z}{\mathrm{DIST}}\right),$$

where C refers to a force or moment coefficient, the subscript *car* refers to the coefficients at the carriage position (either calculated by the IFM or measured in the tunnel), the IFM subscript refers to coefficients calculated by the IFM, and Δz is the distance away from the carriage position. The DIST parameter is a distance from carriage where mutual interference is thought to be unimportant; it is usually set to one store diameter.

Chapter 4

DOMAIN DECOMPOSITION PHILOSOPHY

To generate the detailed computational data required for this study, two computational criteria had to be met:

1. The configuration would have to be modeled as accurately as possible and constructed as easily as possible.

2. Main memory requirements would have to be such that the code could be run with the available memory of the Cray X-MP/12 at the AEDC.

The chimera domain decomposition scheme [7] readily fulfills these requirements. The chimera scheme is a methodology that allows complex configurations to be divided into simpler component parts. The grid of each part can be generated separately, optimized for each topology, and constructed within the required memory restraints (because the computer processes only one grid at a time). The chimera scheme is carried out in a three step process. Once the configuration has been examined to determine how best to partition it, the necessary grids are constructed. During this step, careful consideration must be given to inter-grid communication and mesh resolution. For example, experience has shown that if cell sizes differ by more than approximately a factor of two, the interpolations between overlapping meshes may not be acceptable; the difference in

resolution causes a smoothing effect for data going from the fine to the coarse mesh. Second, the grids must be assembled by a program called PEGSUS (specifically PEGSUS 4.0 [8]) to determine from where to interpolate boundary information and to locate regions of meshes to be deleted from the solution process. When the grids are assembled, some cells of a grid may lie inside the solid body of another grid. Some cells of the wing grid in this configuration will be inside the store, for example. Points such as these need to be located and labeled so that the flow solver will not include them in the solution. In chimera terminology, these unused regions are referred to as holes. Difficulties can also arise when boundary information is required for a fine mesh which creates a hole in a coarse mesh. If a hole is created in a coarse mesh by a smaller fine mesh, the hole may encompass the entire fine mesh, leaving no valid points for interpolation for the fine mesh outer boundary or the coarse mesh boundary enveloping the hole (the hole boundary). The assembly process typically involves some iteration to obtain proper inter-grid communication. Many communication problems can only be solved with the re-creation of the grid or the addition of a new grid. Third, the XMER3D [7] program (here in its Euler flow-solver version) uses the PEGSUS information to calculate the flow-field solution.

4.1 Grid Generation

Grid generation is very often the most difficult and time consuming part of the solution process (as it was in this study). All grids used in this study were algebraic grids constructed with the EAGLE interactive grid generation system [9]. The original EAGLE grid generation system was developed by J.F. Thompson et al. [10], whereas the interactive implementation was developed at AEDC. The interactive nature of the system significantly reduced the time and effort required to construct high quality grids for this study, though it by no means reduced the process to a trivial one (approximately four man-months of effort were required to generate and optimize all the grids). Twenty-six grids were used to model the configuration. Sixteen grids were actually used by the flow solver whereas the remaining ten were used by PEGSUS to more clearly define

hole regions. It should be noted that as the store was placed in the different locations below the pylon, no new grids were required; only the paths of communication had to be redefined. This ease of grid relocation is a major advantage of the chimera scheme over many other schemes currently in use.

4.1.1 Subgrids

Finned Store

The store consists of a tangent-ogive/cylinder/tangent-ogive body with four fins forming a cruciform (see Figs. 1.1, 2.3, and 2.4). Each fin was modeled with a separate grid and contained 32,025 points. The grids (see Fig. 4.1) were constructed with 61 points in the ξ direction, 25 points in the η direction, and 21 points in the ζ direction ($61 \times 25 \times 21$). As an illustration of the difficulties in grid generation, note how the η=1 plane at the root of the fin in Fig. 4.1 conforms to the body of the store. In the chimera scheme, when two grids with solid boundaries are in contact, one of the grids should conform to both solid surfaces. This constraint is necessary in PEGSUS to ensure proper communication at the juncture, and in XMER3D for the implementation of the boundary conditions (see [8]). The EAGLE grid generator aided in this conformal grid construction with routines that specifically address the problem.

The store and sting were composed of five meshes (see Fig. 4.2). The store body was divided into four separate grids, whereas the sting was modeled with a single grid. Each of the four grids on the store contained 75,981 points ($57 \times 43 \times 31$), and the sting grid contained 54,653 points ($41 \times 43 \times 31$). Rather than model the details of additional support hardware, the end of the sting was simply closed off. This simplification was felt to be justified since the end of the sting was over four store lengths downstream from the end of the store and was unlikely to noticeably affect the store solution.

Pylon

The pylon was described with two grids (see Fig. 4.3). The first modeled the pylon from

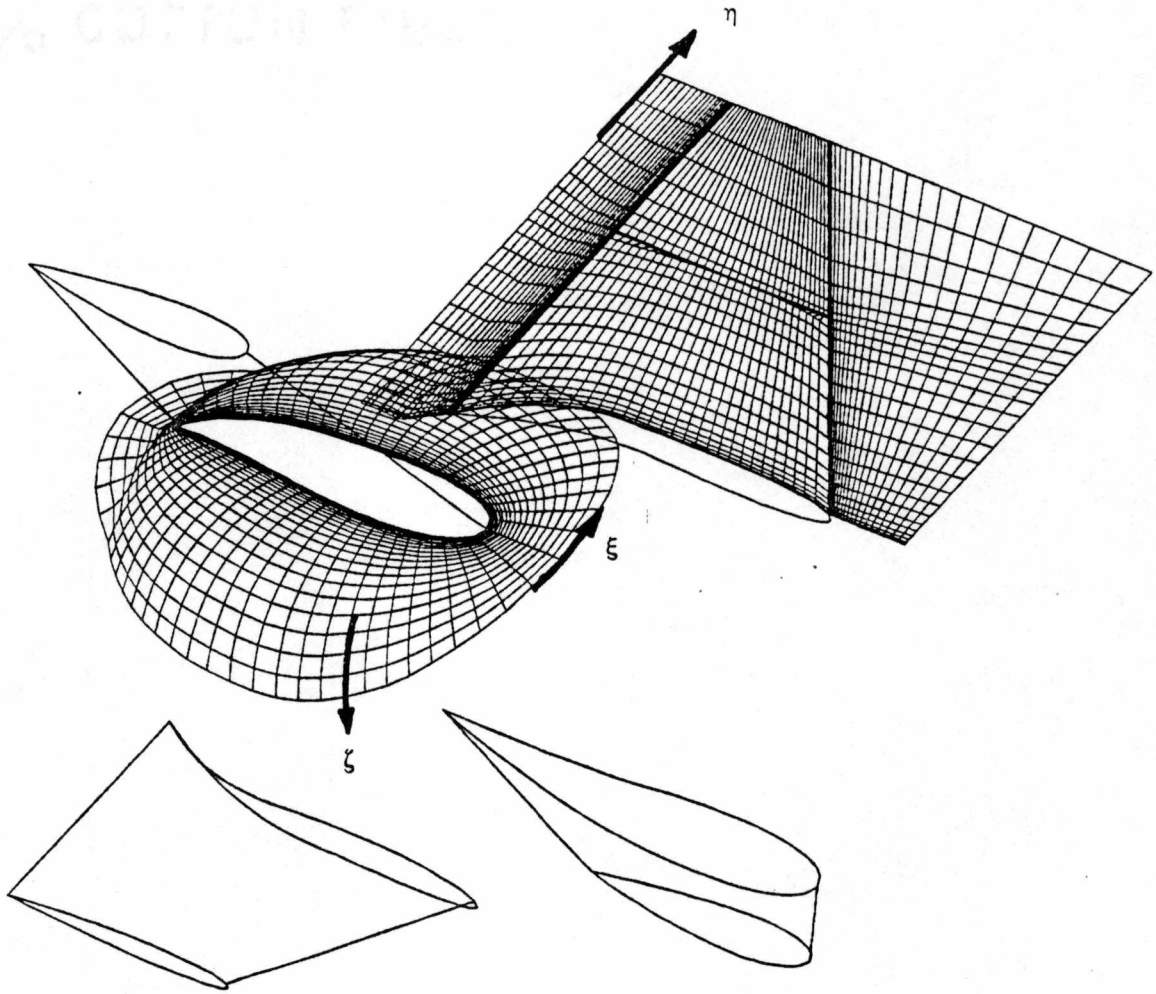

Figure 4.1: Fin grids

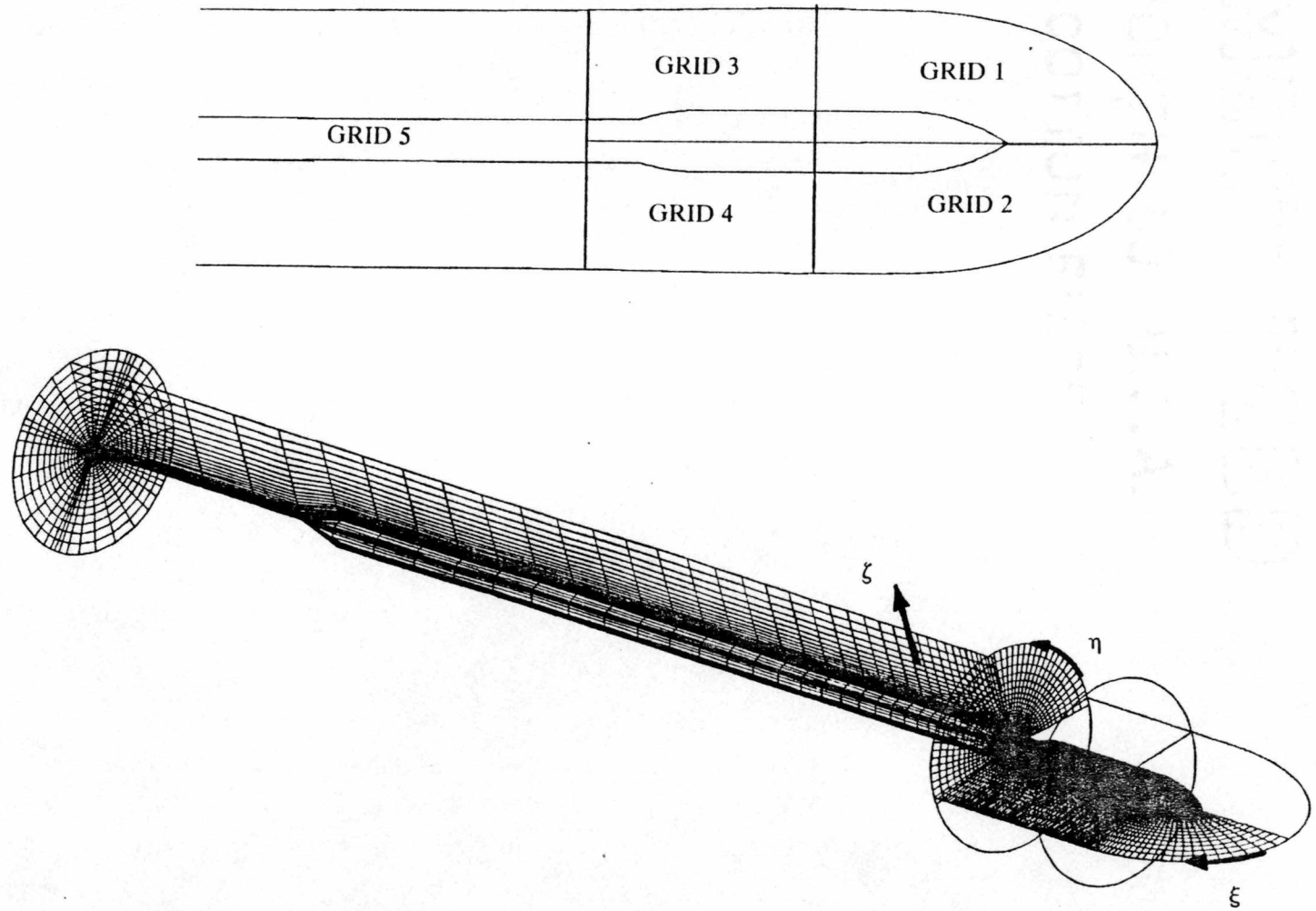

Figure 4.2: Store/sting grids

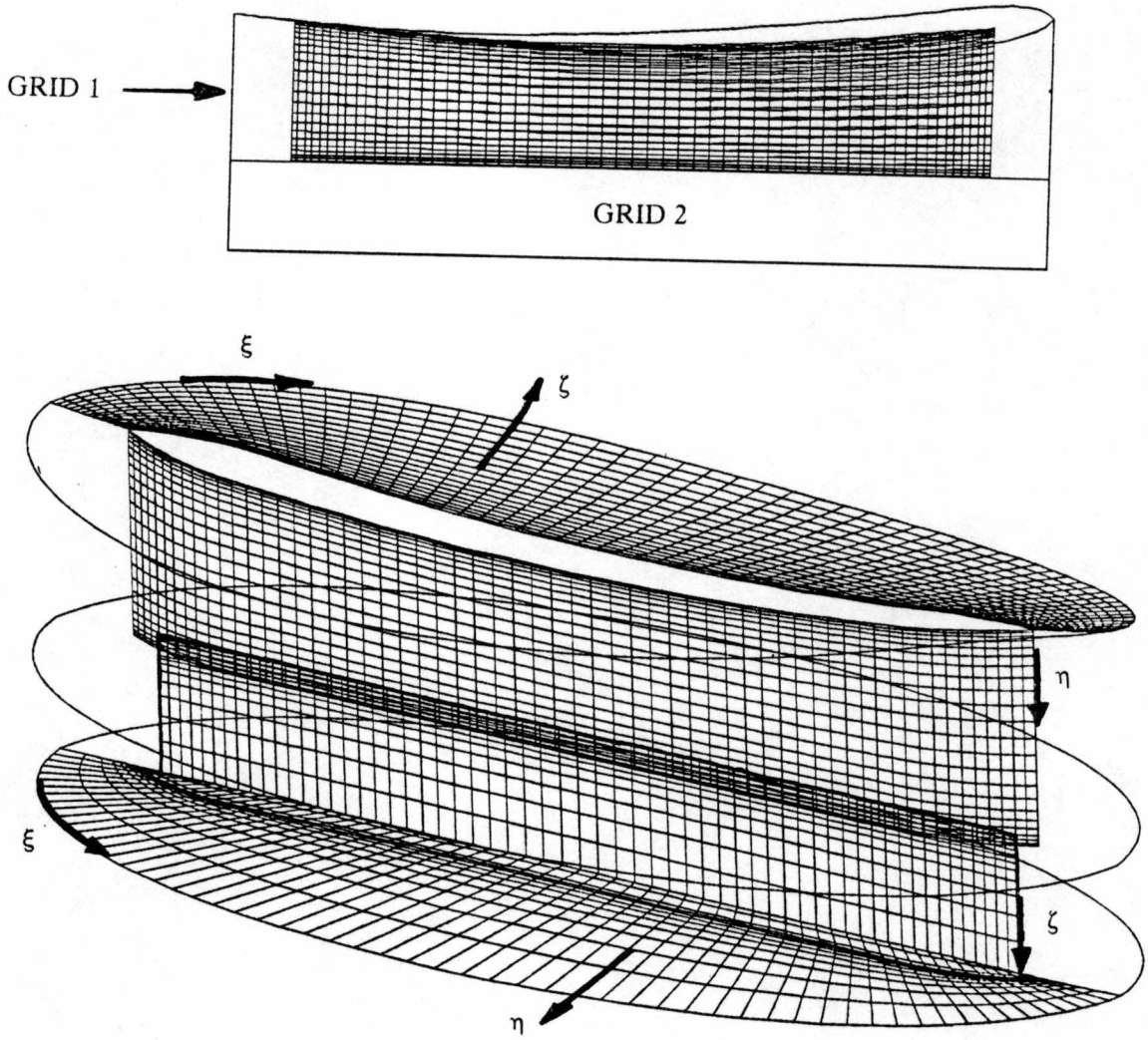

Figure 4.3: Pylon grids

the wing/pylon junction to the edge of the pylon tip. It contained 52,877 points ($121 \times 23 \times 19$). This grid was constructed as an o-grid around the pylon. The second mesh modeled the tip of the pylon and a region extending to one store diameter underneath the pylon. This second mesh contained 75,625 points ($121 \times 25 \times 25$). The second mesh was constructed by taking the constant η plane at the tip of the first mesh, filling the ungridded area where the body of the pylon had been, and reproducing the resulting plane for all 25 ζ=constant planes.

Wing

The wing was also described with two grids (see Fig. 4.4), both of which were o-meshes. The first extended from the vertical tunnel symmetry plane to 3.10 store body diameters past the pylon. It was composed of 79,375 points ($127 \times 25 \times 25$). The second overlapped the first and extended out past the wingtip 3.35 store diameters. It contained 66,675 points ($127 \times 21 \times 25$). The sting for the wing at the vertical symmetry plane was not modeled. It was felt that the sting was far enough away from the pylon location (6.5 store diameters) to ignore the sting effects.

Aerodynamic Wind Tunnel (4T)

A single Cartesian grid was used to model the wind tunnel walls (see Fig. 4.5). The tunnel grid extended from 16.83 store lengths upstream of the leading edge of the wing to 9.43 lengths downstream. This grid was constructed with 79,625 points ($65 \times 35 \times 35$). It is virtually impossible to model the tunnel wall porosity in the grid, therefore, porosity was modeled with boundary conditions as described in Section 4.3.2.

Communication Grids

Two of the grids used did not model any physical boundary on the configuration. They were constructed to aid in communication among the dissimilar sized cells of some of the grids. A grid was constructed to help communication between the store grids and the tunnel grid (see Fig. 4.6). It was a cylindrical mesh that loosely followed the outer cells of the store meshes. This grid

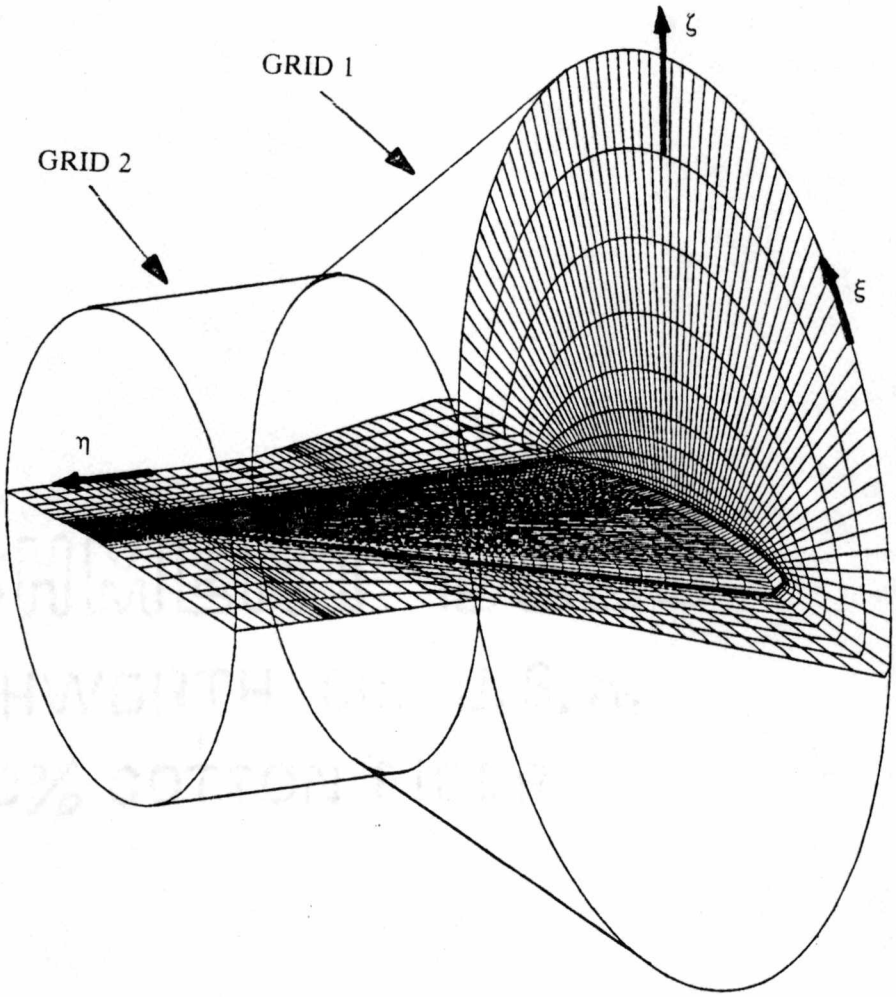

Figure 4.4: Wing grids

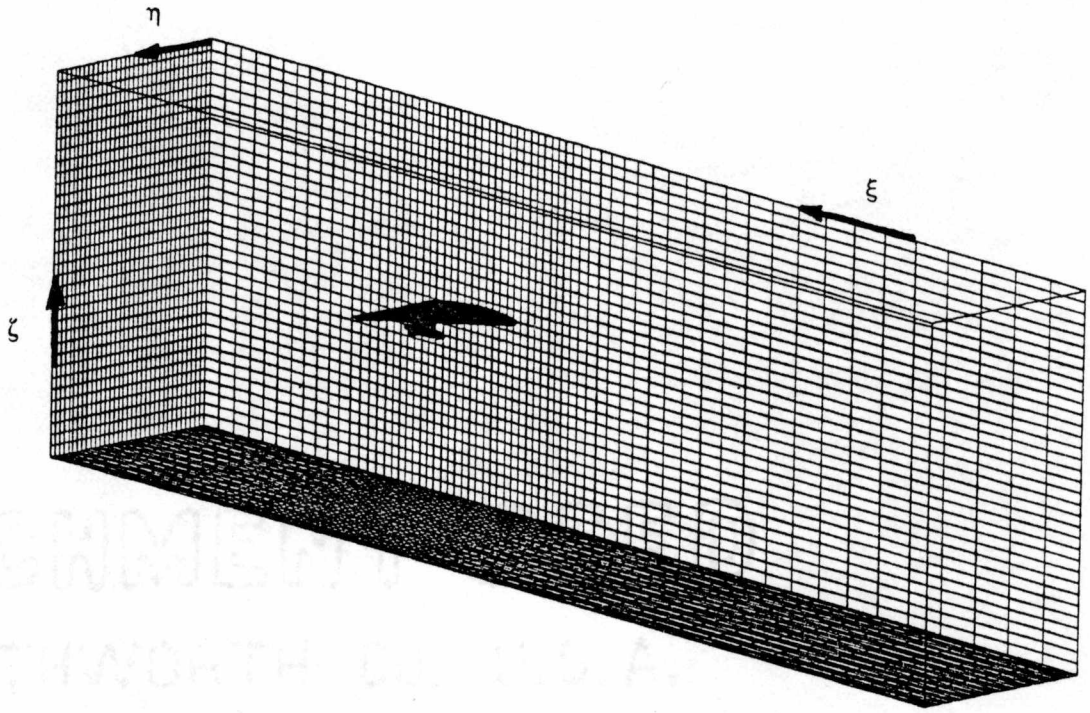

Figure 4.5: Aerodynamic Wind Tunnel (4T) grid with wing/pylon/store superimposed

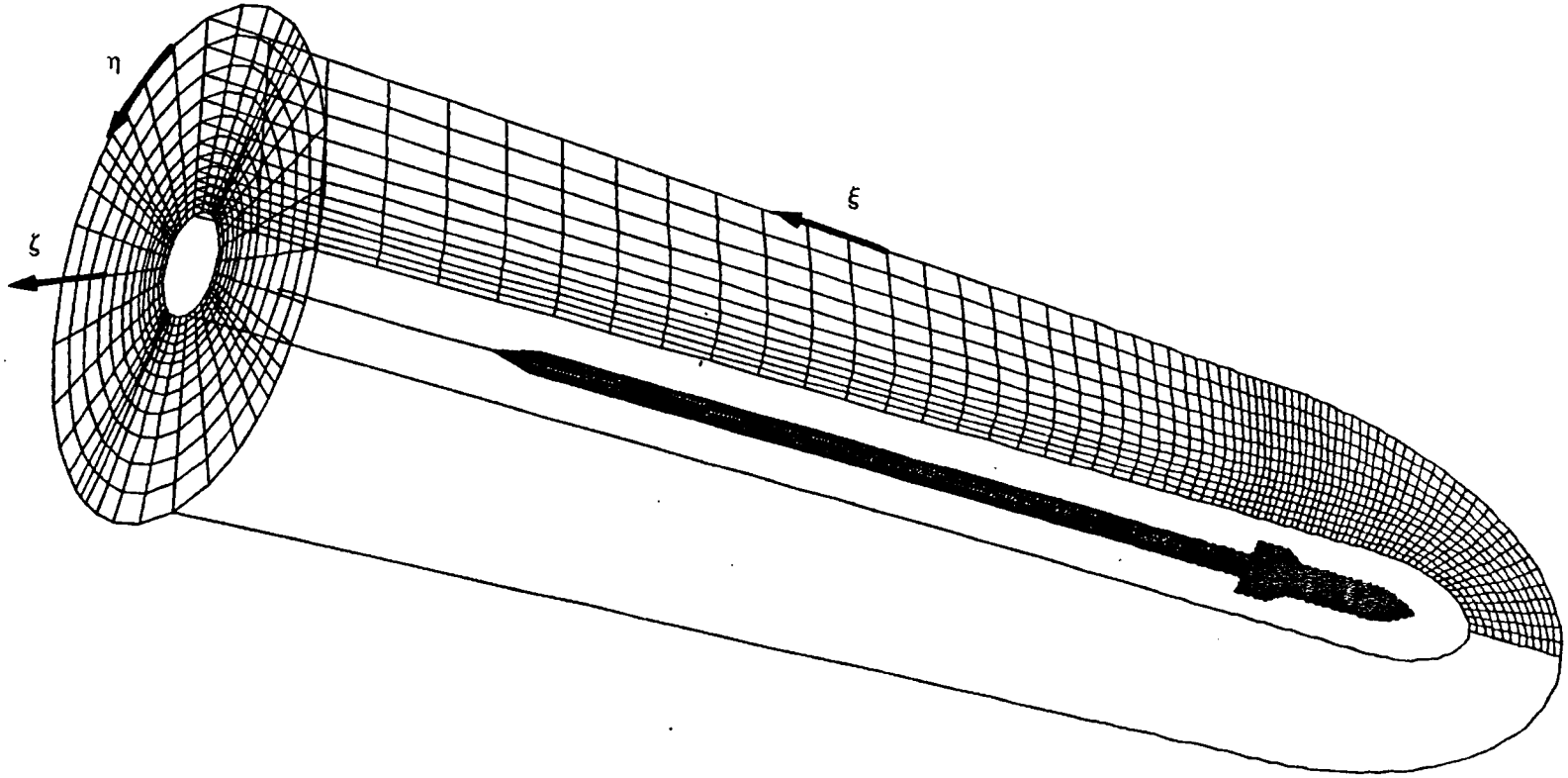

Figure 4.6: Store communication grid with store/sting superimposed

was constructed of 39,689 points ($71 \times 43 \times 13$). The other communication grid was a Cartesian grid that was intended to help interpolation primarily among the wing grids and the tunnel grid (see Fig. 4.7). It contained 41,943 points ($33 \times 41 \times 31$).

Hole Grids

The remaining grids were used only by PEGSUS to better define hole regions and the associated paths of communication. These so-called "hole grids" were necessary for three reasons (see also [8]):

1. As was stated before, passing high gradient information from a fine mesh to a coarse mesh should be avoided because of resolution problems. Therefore, when a fine mesh creates a hole in a coarse mesh, it is desirable to create a hole in the coarse mesh so that the cell sizes are less dissimilar (cell volumes typically increase as the distance from the body surface increases).

2. PEGSUS often has difficulties creating holes using a boundary with very sharp corners (at the the store nose or the wing trailing edge, for example); spurious hole points appear.

3. The hole region must be completely enclosed or extra hole points will be created through the opening. For example, in Fig. 4.2, if the $\zeta=1$ surface of the sting were used to create a hole, hole points upstream of the sting would be created because the $\zeta=1$ surface at the inflow plane of the grid is not closed off.

For completeness, then, a hole grid was needed: (1) for each of the fins, (2) for the store to make a small hole in the pylon grid, (3) for the store to make a large hole in the wing and tunnel grids, (4) for the pylon to make a hole in the store and wing grids, (5) for the wing to make a hole in the tunnel grid, (6) for the wing to make a small hole in the store and store communication grids, and (7) to remove part of the store communication grid that extended past the symmetry plane. This last hole grid was necessary because the store communication grid (see Fig. 4.6) was too large to fit completely on one side of the symmetry plane.

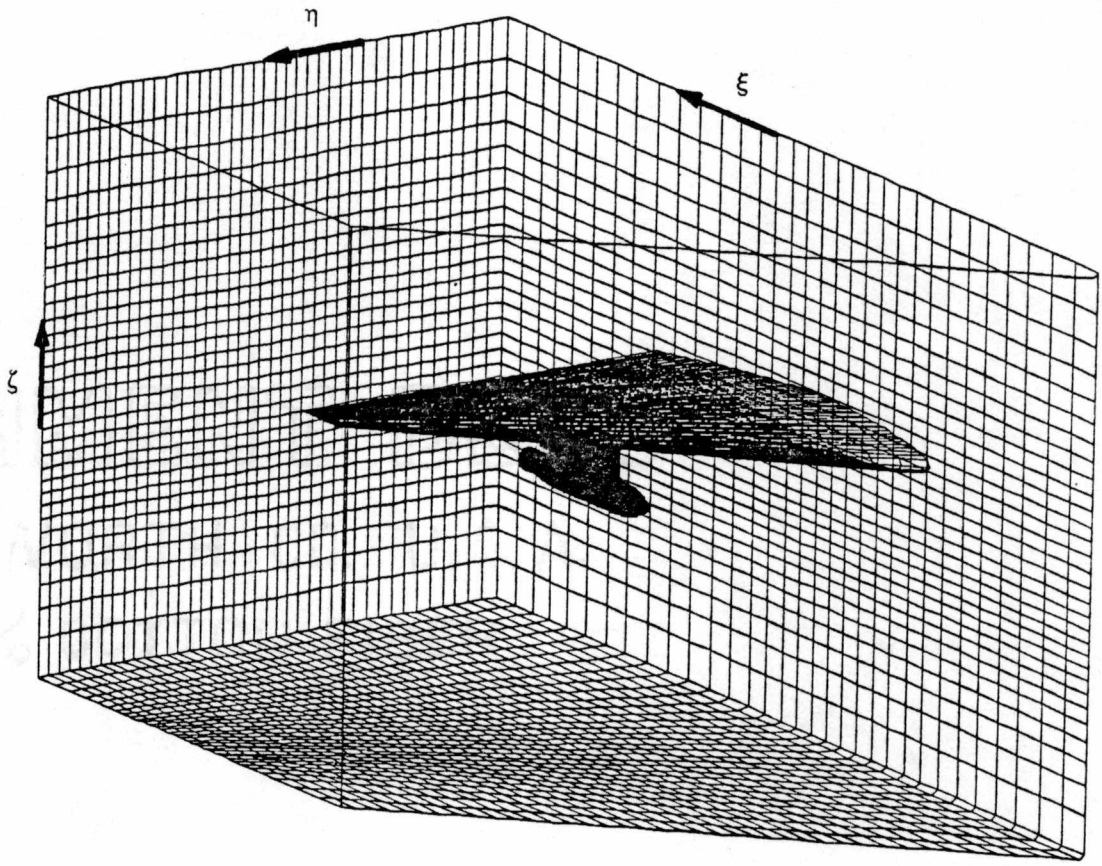

Figure 4.7: Wing communication grid with wing/pylon/store superimposed

4.2 Inter-grid Communication

The PEGSUS code has two primary functions: (1) locate and label hole points, and (2) identify the cells to be used for interpolating flow variables for the hole and outer boundaries.

In addition to the previously discussed problem of locating holes, the outer boundary points of a mesh contained inside another require information from the nearby points in the enveloping mesh; otherwise, one component of the configuration will never affect the flow field of the others. Conversely, points in the enveloping mesh near the hole will require information from nearby points in the inner mesh. This information is calculated by PEGSUS and subsequently written to a file to be used by the flow solver, XMER3D.

4.3 Solving the Euler Equations

4.3.1 General

The flow solver, XMER3D [7], solves the three-dimensional Euler (or thin-layer Navier-Stokes equations) using the Pulliam and Steger implementation [11] of the Beam and Warming approximate factorization algorithm [12]. To begin the solution, some initial conditions must be set at every point in the grid. For the initial calculations, conditions were set to free-stream conditions, but some of the later calculations used a previous solution with a different store position for the initial conditions, which approximately halved the number of time steps required for convergence. After the initial conditions have been set, the iteration process begins. A time iterative procedure is used to calculate the flow field. First, XMER3D explicitly imposes the physical boundary conditions on a given mesh and marches the solution on that mesh forward one time step. The interpolated boundary values for the mesh are then computed and imposed; the location of the values to be used in the calculation were previously determined by PEGSUS as described above. This sequence is repeated on each successive mesh. The entire procedure is then repeated until some convergence criteria are met. For this study, the solution was assumed to have converged once the calculated forces did not change by more than approximately 1.0×10^{-3} over 50 iterations.

Convergence typically occurred between 600 and 700 time steps and required approximately 10 CPU hours on the AEDC Cray X-MP/12 for cases starting from free-stream conditions.

4.3.2 Boundary Conditions

In XMER3D, all boundaries of all grids must have some boundary condition imposed. Some of the boundary conditions will be imposed by interpolations defined by PEGSUS. Many, however, must be explicitly imposed by boundary condition subroutines.

On all solid surfaces, the velocity normal to the surface was set to zero, and a zeroth order extrapolation was used to determine pressure and density. Velocity, density, and pressure were then used to calculate the total energy.

For surfaces that extended past the solid boundaries on the wing tip and fins, the flow variables at the points on either side of the surface were averaged. At the wing and fin tips, the flow variables above, below, and one point outboard were averaged with the old value. In the second pylon mesh along the pylon centerline plane, the two values at the point plus the values on each side were simply averaged (see Fig. 4.3).

The edge line values on the pylon tip were calculated by averaging the flow variables at the seven adjacent points not inside the pylon on the same ξ surface.

The trailing edge velocities for the fins, the wing, and the pylon were calculated by averaging from the values upstream and downstream, and then averaging the two values at the overlap region. The density was not modified. The total energy was then calculated by assuming constant total enthalpy.

The flow variables on the polar axes were averaged from the adjacent points not on the axes.

A vertical symmetry plane was assumed at the tunnel centerline. An additional surface was added beyond the symmetry plane of the wing and tunnel grids and was treated as a reflection plane to the surface inside the symmetry plane. Thus, zero flow through the symmetry plane was enforced.

The inflow boundary condition for the tunnel was determined by using the Riemann Invariants [13] according to the formulation of Jameson, et al. [14].

Outflow $\rho, \rho u, \rho v$, and ρw values were determined by a zeroth-order extrapolation from values upstream. The energy was determined by assuming constant total pressure. In the early phases of this study, attempts were made to implement a characteristic outflow boundary condition which used Riemann Invariants. However, stability problems were encountered with the characteristic boundary condition so the zeroth order extrapolation routine was used instead. Experience of the author's colleagues had shown that the extrapolation routine was more stable and the error introduced would probably be small.

The porous wall boundary conditions on the tunnel walls are based on a method developed by J.L. Jacocks and reported in [15]. The routine uses empirical correlations and the local boundary layer displacement thickness to specify the flow variables on the tunnel walls.

In addition to the boundary conditions described above, a boundary condition was required for all boundary points for which PEGSUS could find no suitable interpolation points (orphan points). In XMER3D, orphan points are not automatically updated, therefore the flow variables at these points must be set to some value or else remain at free-stream conditions. The procedure used was to simply average the six values adjacent to the point along with the current value at the point.

Chapter 5

RESULTS AND DISCUSSION

As stated earlier, seven solutions were completed, all of which are listed in Table 1.1. Initially, plans were made to obtain solutions only for cases 1-5. However, when those calculations were completed, it was found that agreement between CFD and IFM predictions was very poor. Cases 6 and 7 were then deemed necessary for more complete information.

Calculated pressure distributions along the length of the store at four azimuthal locations on the store body (with ϕ defined in Fig. 2.4), as well as the fin pressure distributions at 40% span are included for cases 2-7. Force and moment coefficients calculated by CFD and the IFM are also presented for all positions. Tunnel pressure and load data were available for the store at only the carriage position (case 2), the trajectory position (case 7), and at zero incidence in a free-stream flow (from an earlier test). Data are compared to the pertinent calculations.

Pressure distributions for the store at the carriage position are shown in Fig. 5.1. The agreement between the data and calculations is surprisingly good considering that no viscous effects were modeled. Typical trends for inviscid calculations representing real, viscous flows are apparent; i.e., in the calculations, shocks are shifted downstream and pressure changes are more peaked compared to the data. As one would expect, the agreement is poorest between the store and pylon at the ϕ=5 degree location (see Fig. 2.3 and 2.4) since, in the test, viscous effects are very significant in this region. The calculations predicted a double expansion and compression of

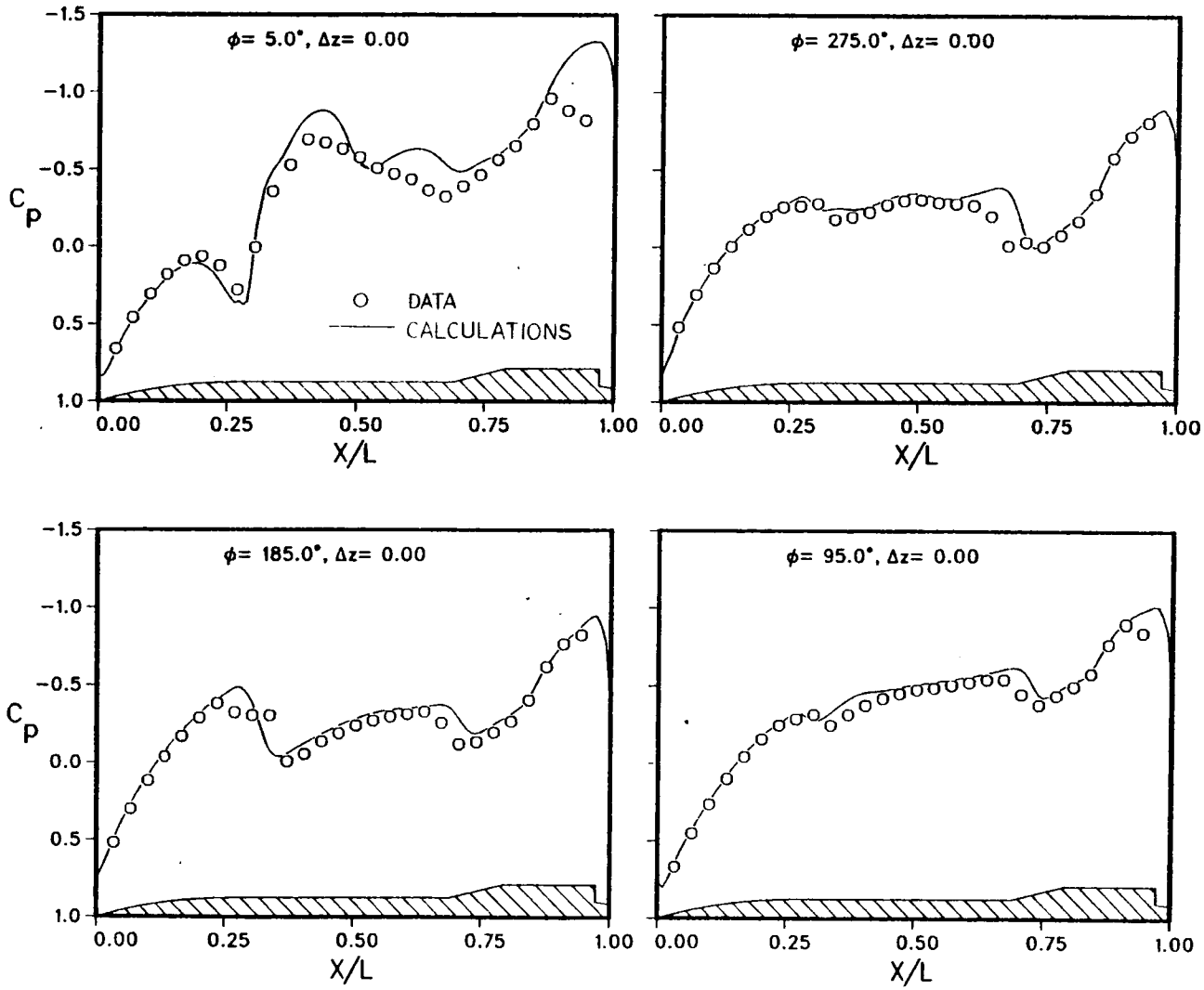

Figure 5.1: Pressure coefficient distribution at the carriage position
a. Body distributions

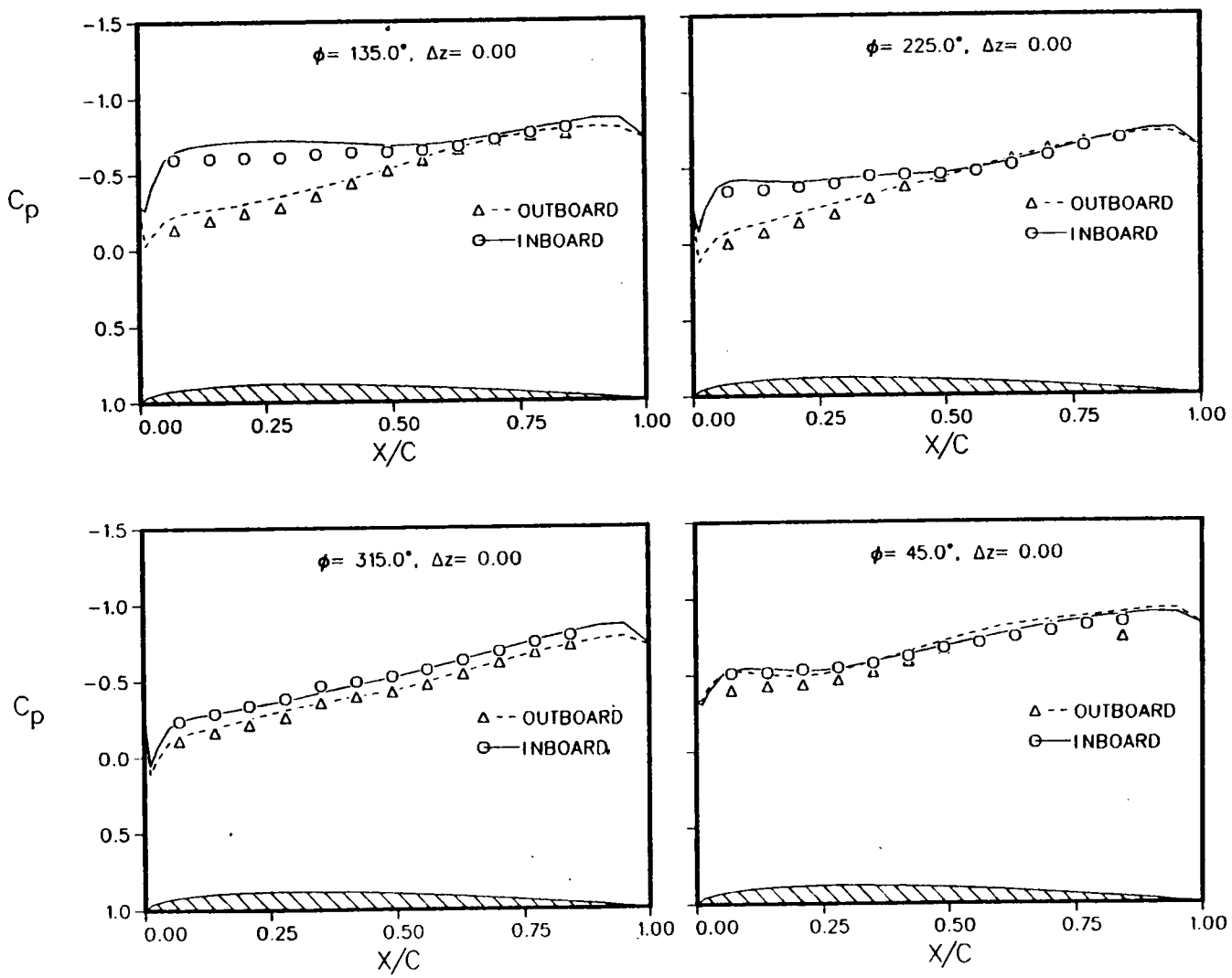

Figure 5.1: Concluded
b. Fin distributions

the pressure that is greatly exaggerated compared to the trend obtained in the tunnel test. The agreement improves as ϕ approaches the 180 degree location away from the pylon. The asymmetry of the pressure distribution between the ϕ=95 and 275 degree locations is caused by the crossflow created by the delta wing. The plateau in the 185 degree data between x/L=0.25 and x/L=0.30 may be caused by crossflow separation or transition from laminar to turbulent flow, both of which are viscous phenomena and are neglected in the Euler solutions. Agreement is also very good on the fins. It was expected that the viscous interaction between the pylon and fins would result in a larger difference between the data and calculations than was encountered.

Figures 5.2– 5.5 are plots of pressure distributions obtained from calculations placing the store with zero pitch, yaw, and roll angle at locations directly below the carriage position; 0.25, 0.50, 1.0, and 4.0 store diameters , respectively. The trends of the pressure curves indicate movement toward free-air flow as the distance from the pylon increases, which would be expected as the mutual interference effects are reduced. For comparison, pressure distributions calculated on the body for all four locations are shown in Fig. 5.6 along with free-stream data obtained from a test conducted in the Aerodynamic Wind Tunnel (4T) in 1986. Clearly, the large difference between the one and four diameter case indicates that the assumption that mutual interference ends at one diameter is not valid for this configuration.

Force coefficients were obtained from the CFD computations by integrating the product of the pressure at each point by the area of the grid associated with that point. Moment coefficients were obtained by multiplying the calculated force by the distance of the point from the store's c.g. A comparison of the calculations to the data and coefficients predicted by the IFM are given in Table 5.1. Since the body and fins were composed of several grids, forces and moments on the store body and fins were calculated separately. Some interesting information resulted from this integration of separate parts in that it was found that the fins were responsible for typically 50% of the total aerodynamic forces.

The IFM predictions in this study used 11 segments and the flow angles associated with

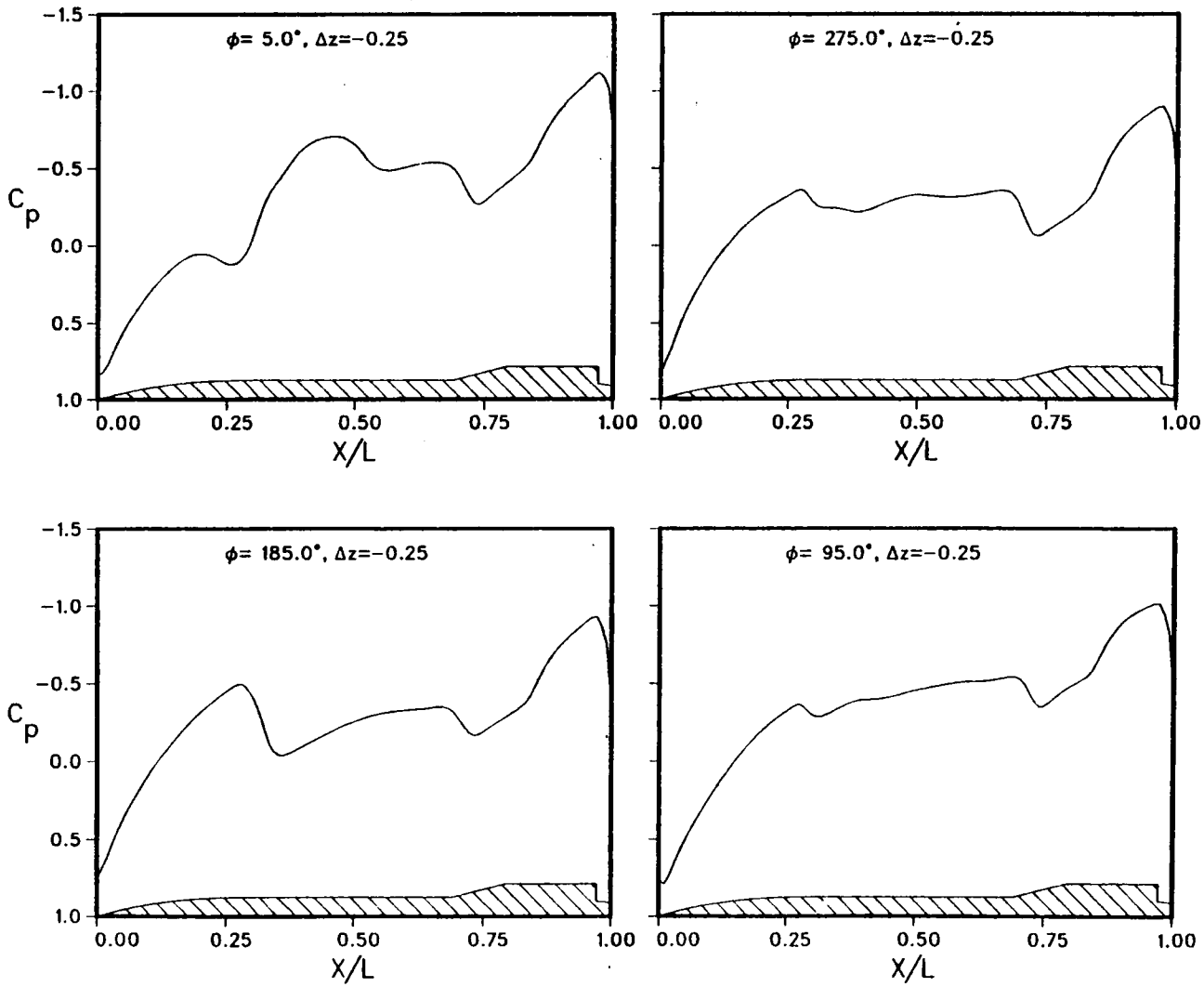

Figure 5.2: Pressure coefficient distribution at Δ z=-0.25
a. Body distributions

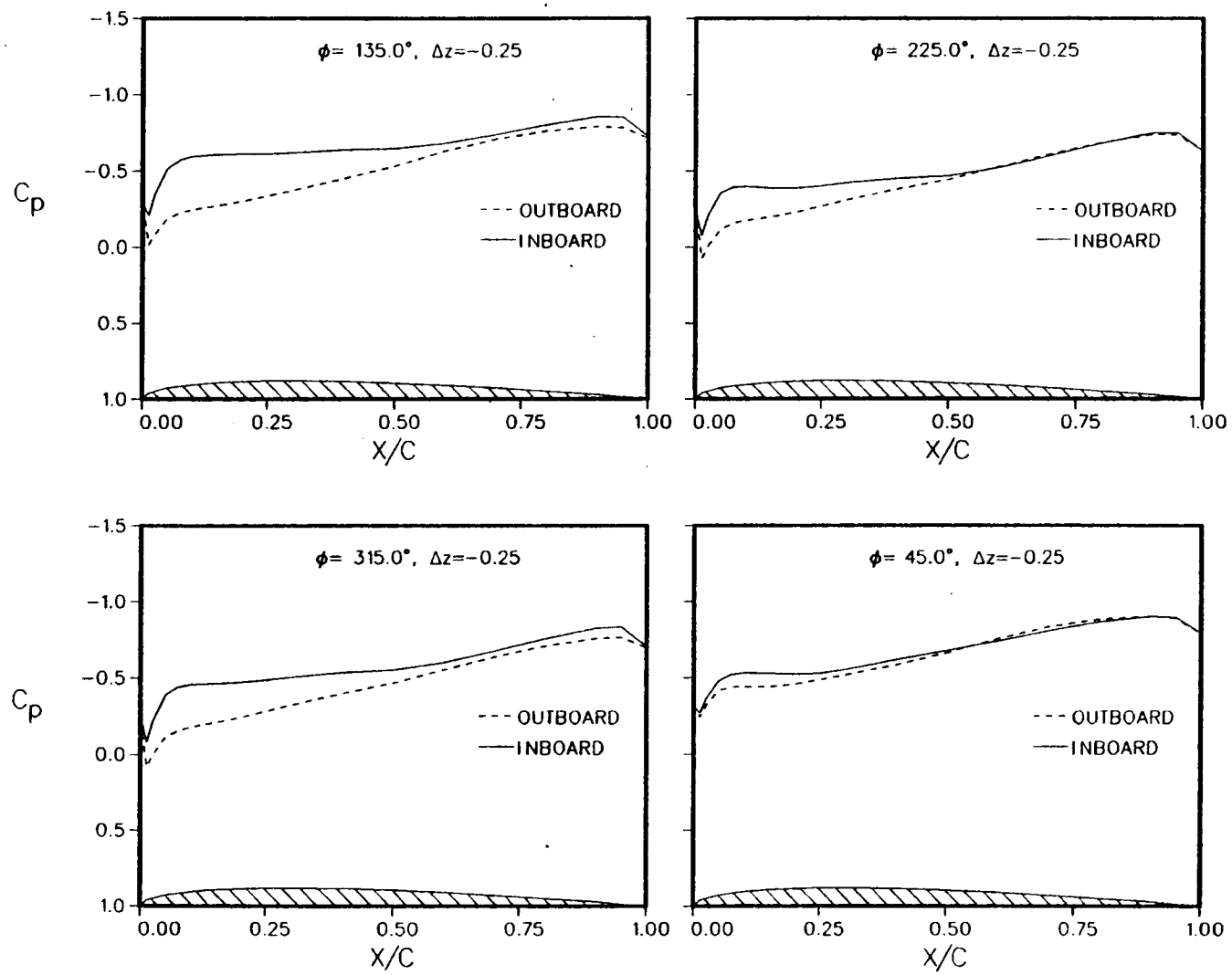

Figure 5.3: Concluded
b. Fin distributions

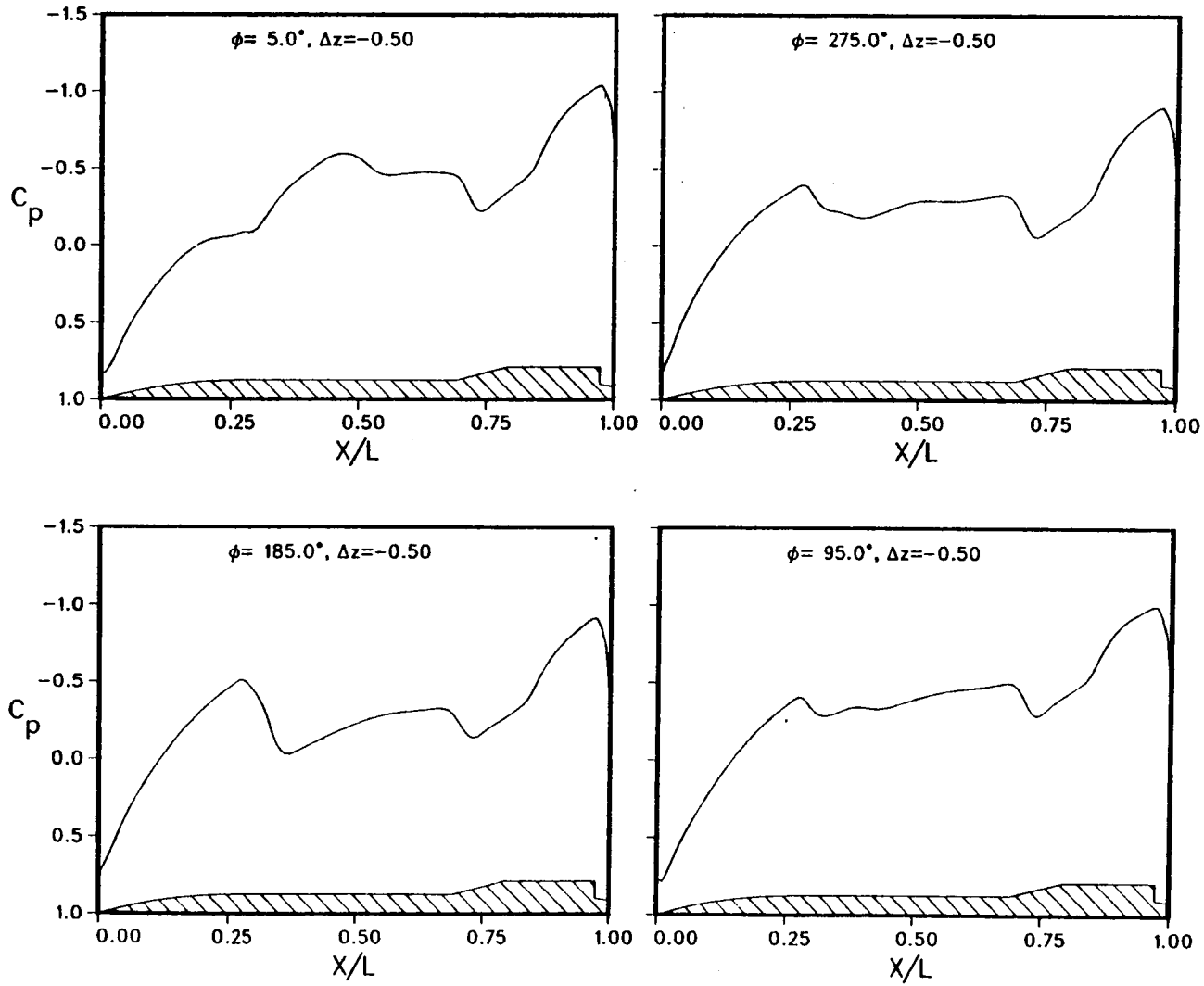

Figure 5.3: Pressure coefficient distribution at Δ z=-0.50

a. Body distributions

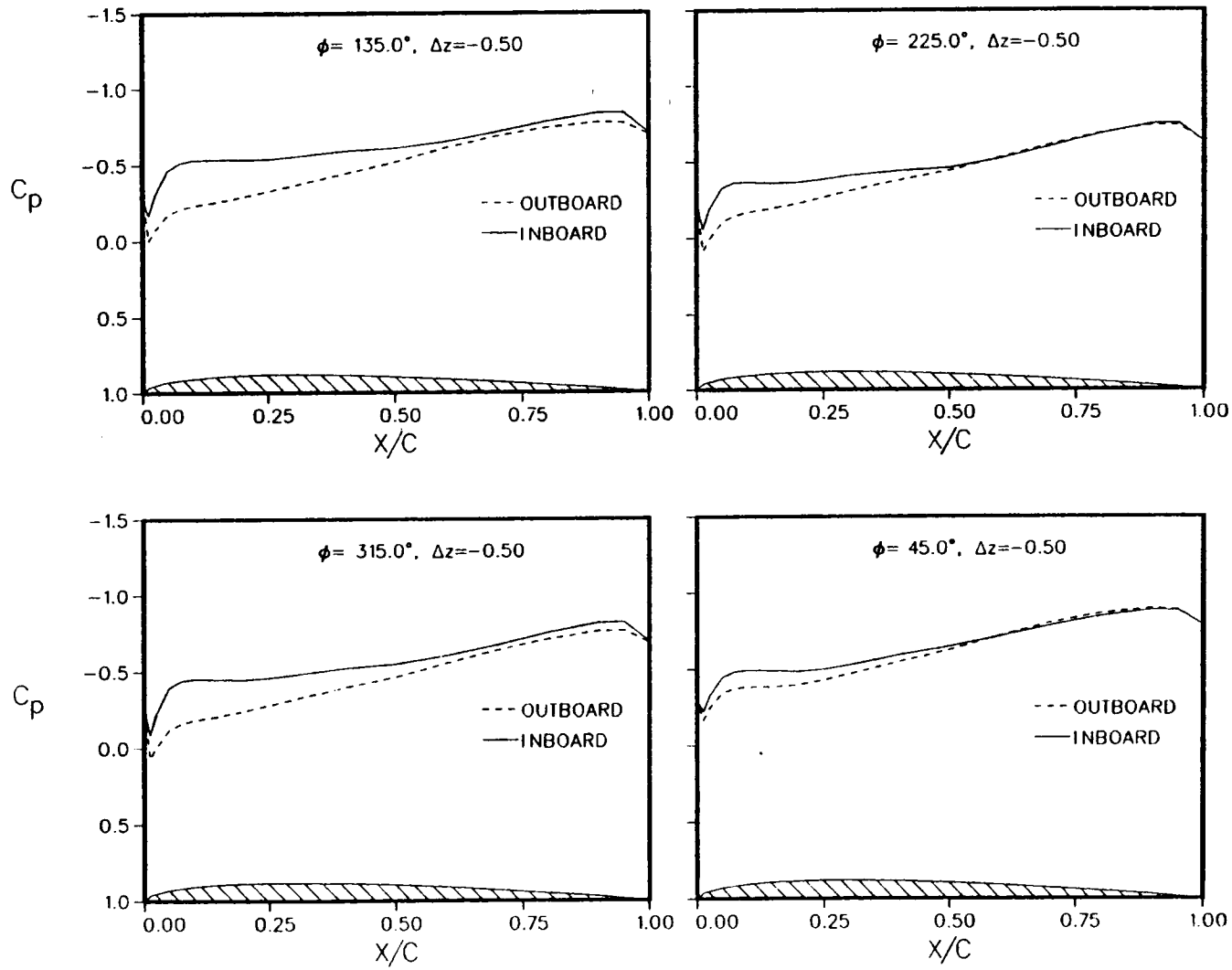

Figure 5.3: Concluded
b. Fin distributions

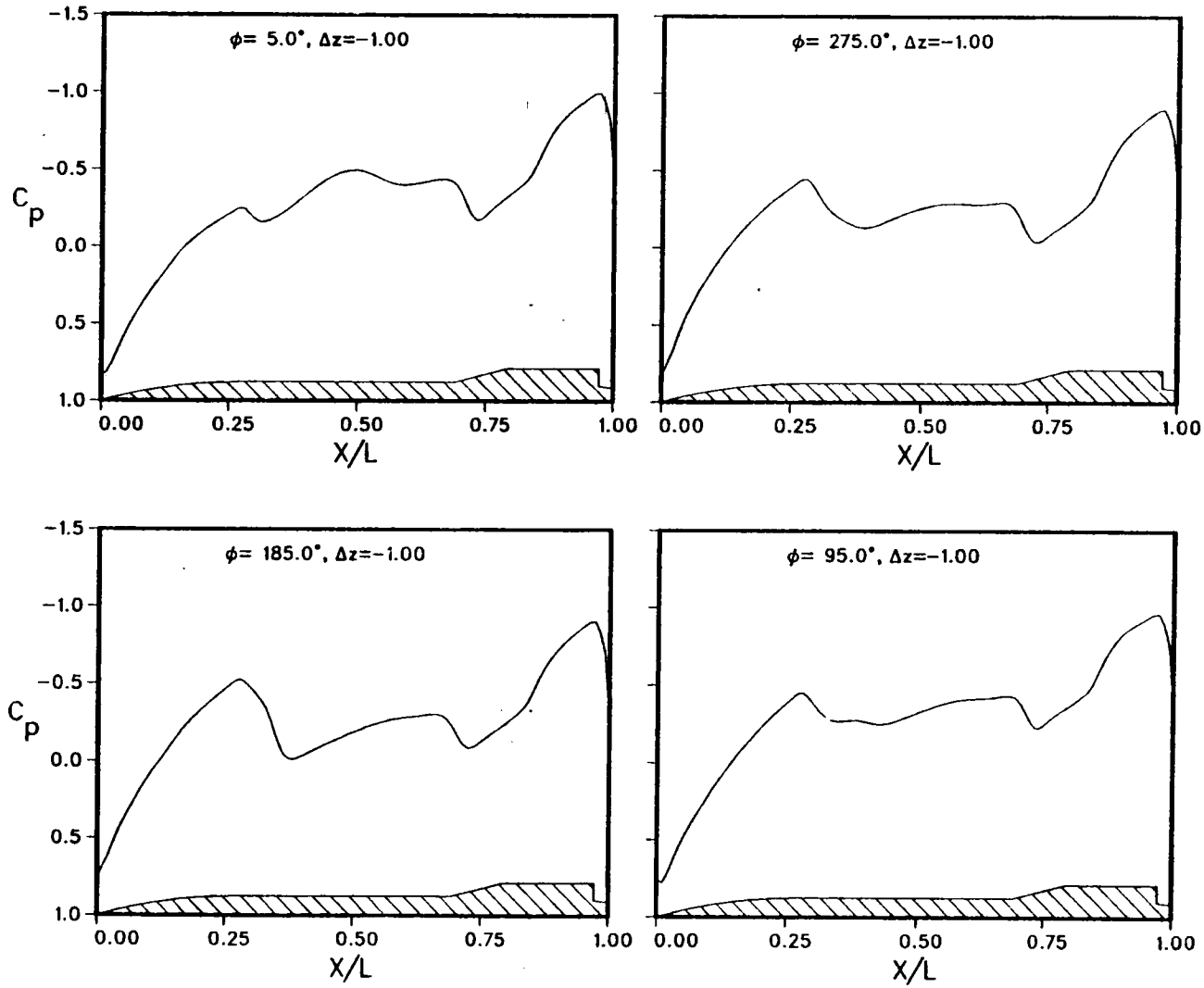

Figure 5.4: Pressure coefficient distribution at Δ z=-1.00
a. Body distributions

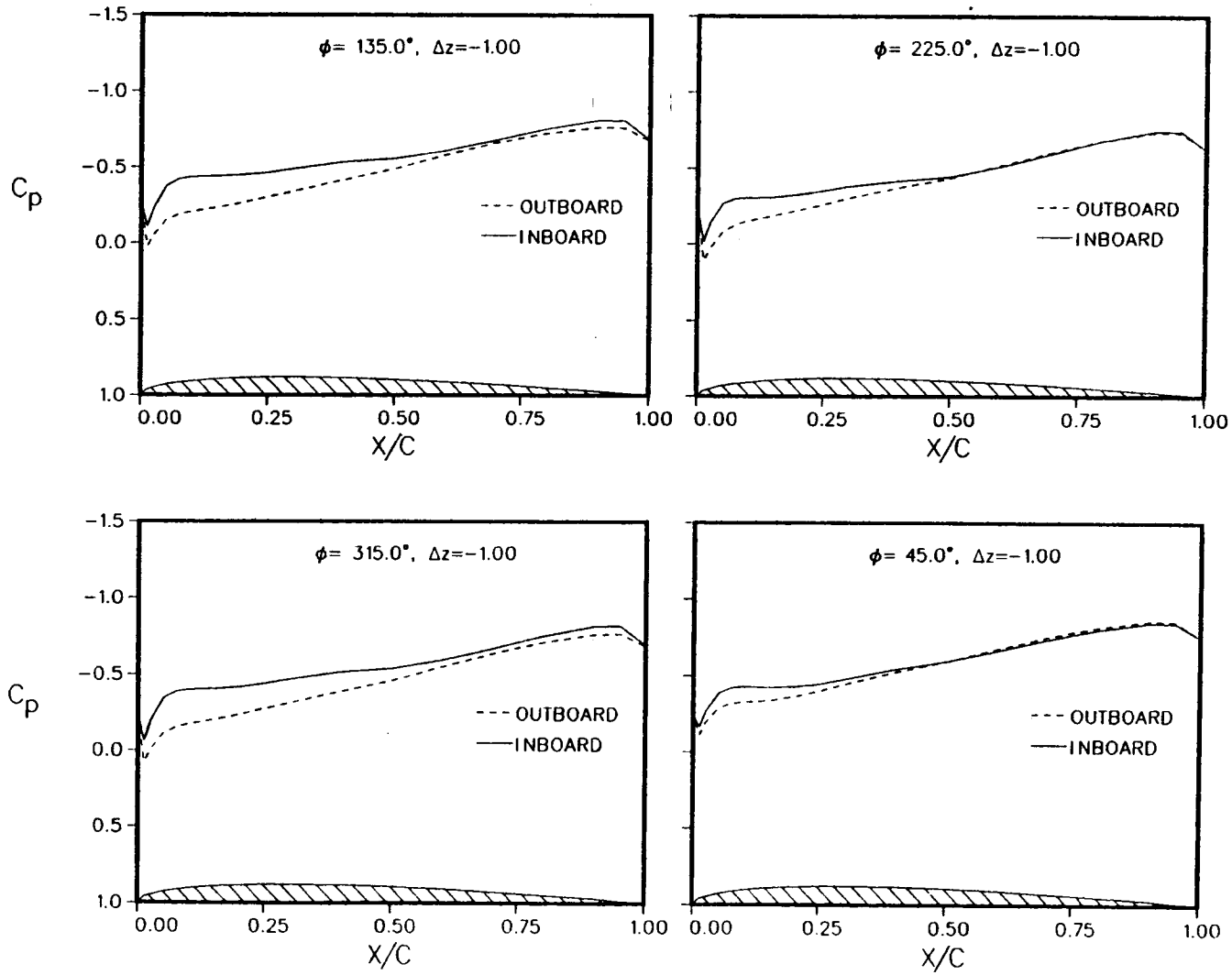

Figure 5.4: Concluded
b. Fin distributions

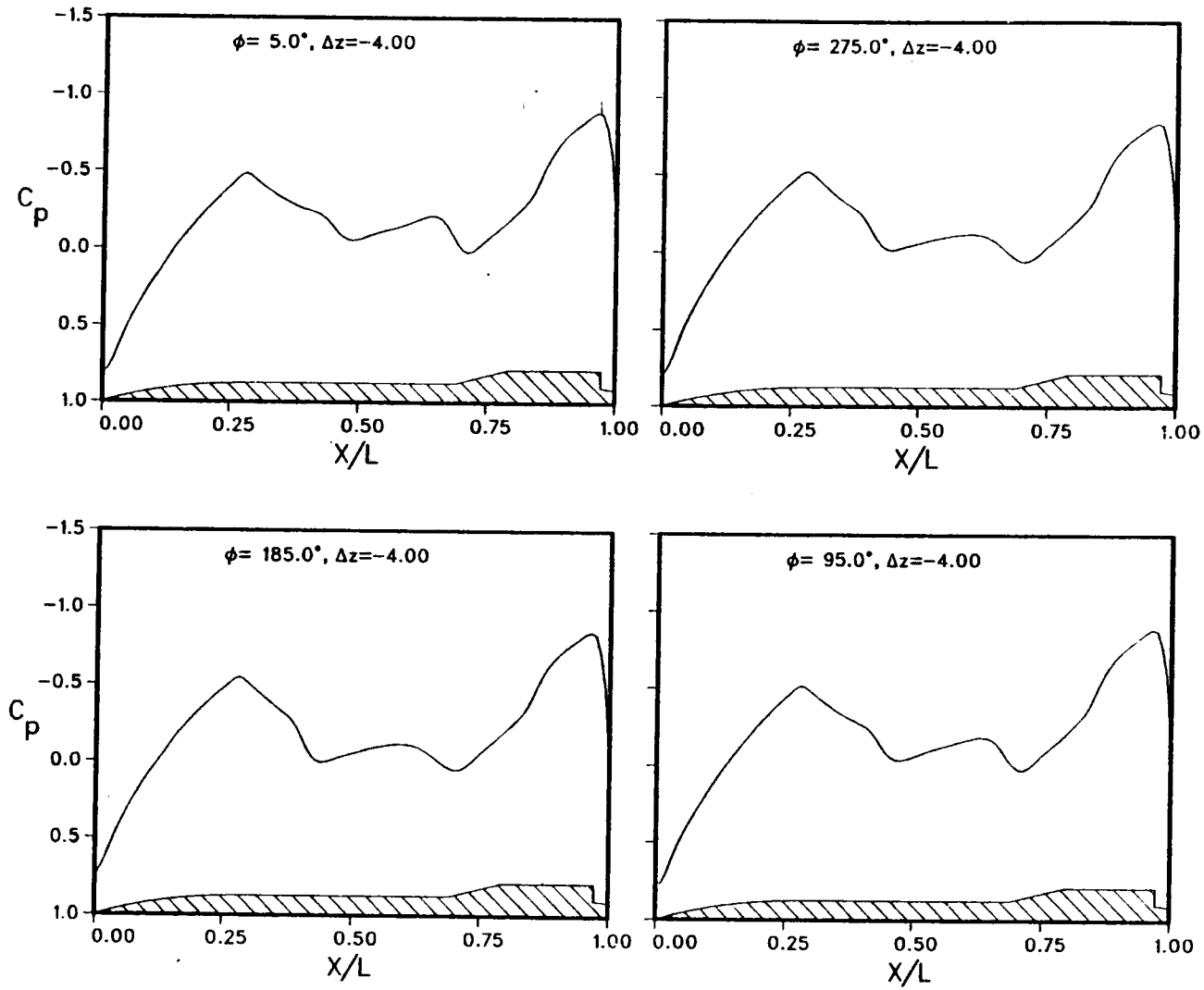

Figure 5.5: Pressure coefficient distribution at Δ z=-4.00
a. Body distributions

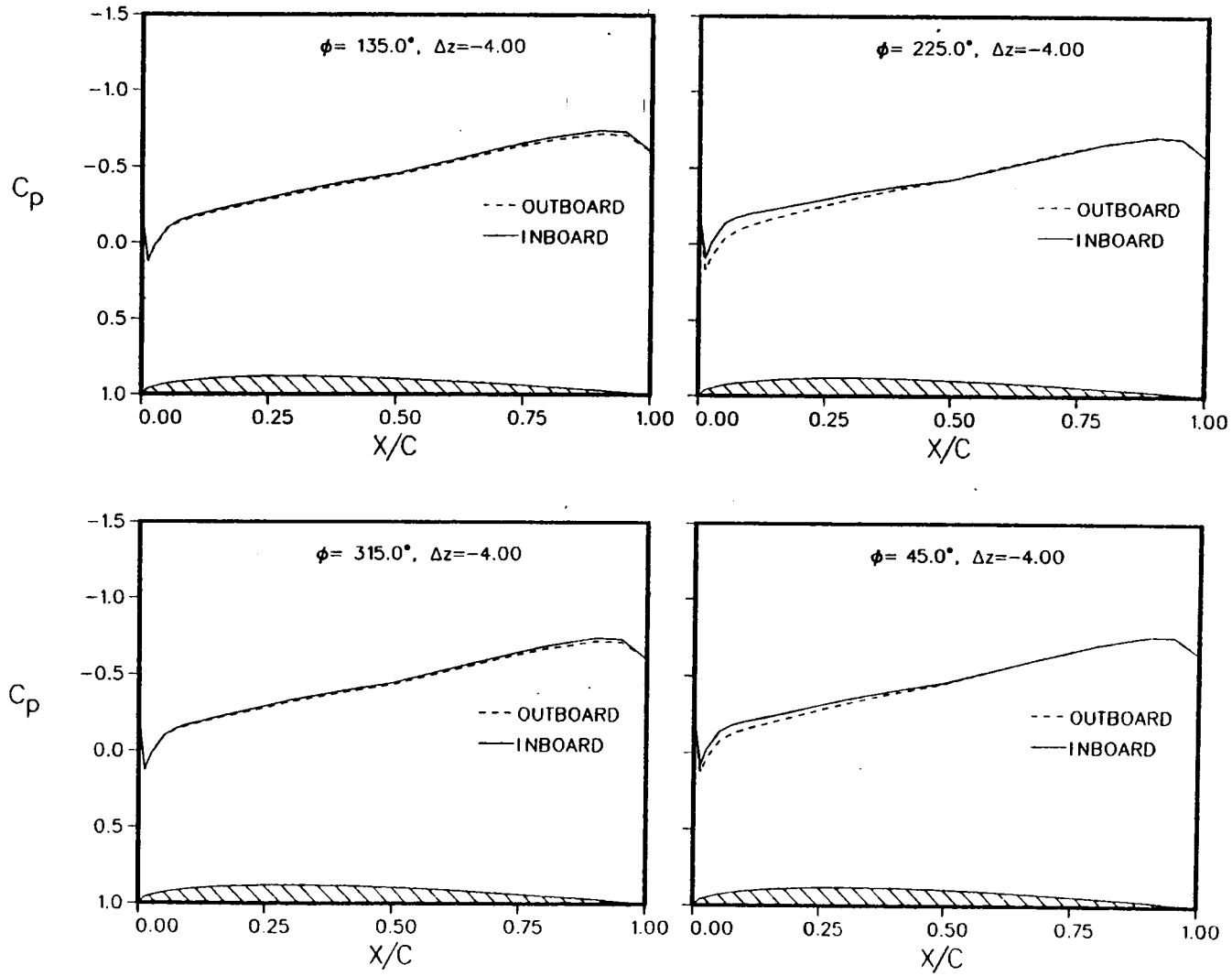

Figure 5.5: Concluded
b. Fin distributions

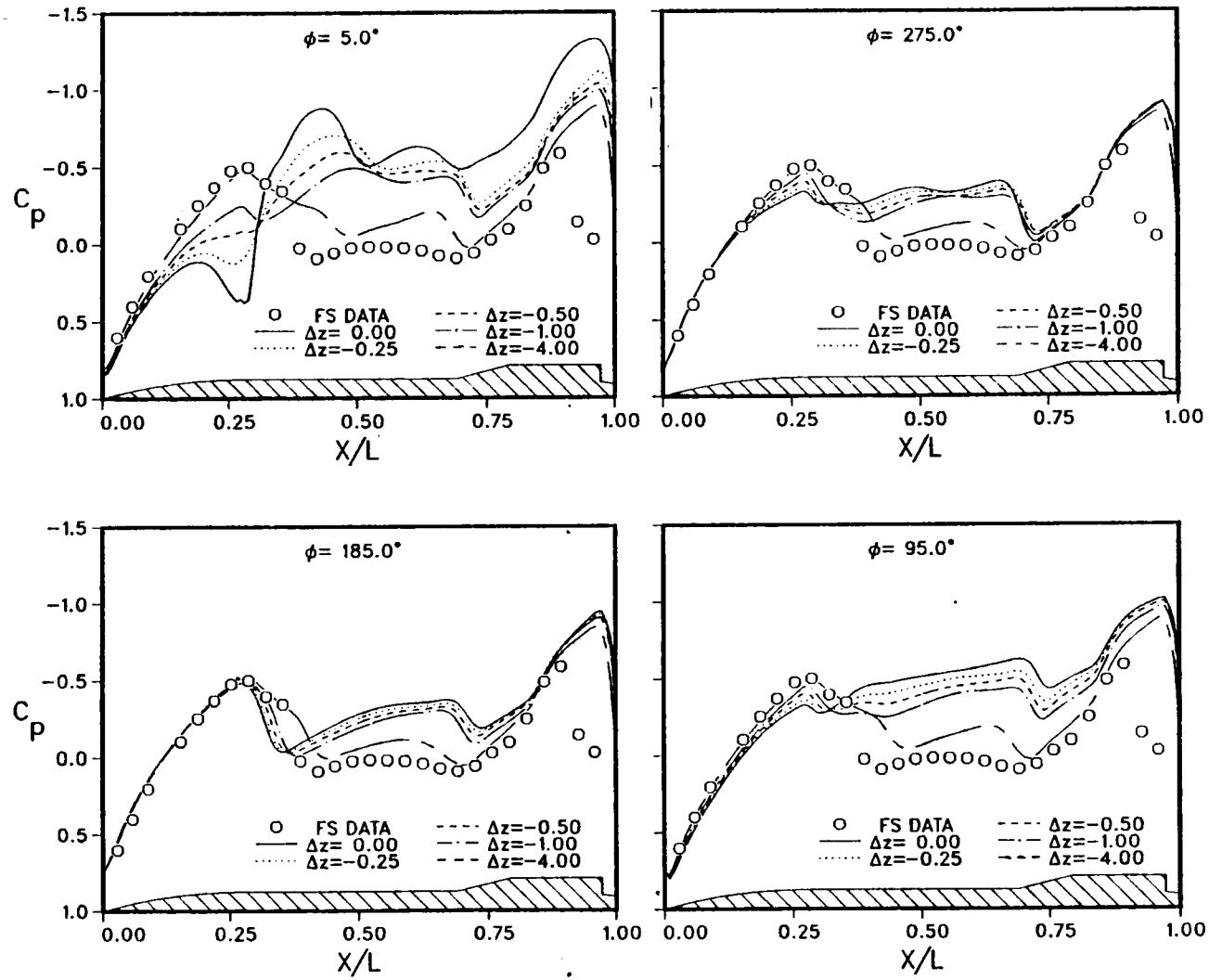

Figure 5.6: Comparison of pressure coefficient distributions

Table 5.1: Force and moment coefficients

		C_N	C_Y	C_m	C_n	C_l	Δx	Δy	Δz	Yaw	Pitch	Roll
CASE 2	CFD IFM DATA	0.660 -0.038 0.644	-0.939 -0.156 -0.954	-1.609 -0.524 -1.430	-1.553 -0.609 -1.520	-0.128 NA -0.100	0.000	0.000	0.000	0.00	0.00	0.00
CASE 3	CFD IFM DATA	0.503 -0.057 NA	-0.751 -0.116 NA	-1.282 -0.458 NA	-1.265 -0.504 NA	-0.070 NA NA	0.000	0.000	-0.250	0.00	0.00	0.00
CASE 4	CFD IFM DATA	0.409 -0.064 NA	-0.642 -0.092 NA	-1.099 -0.401 NA	-1.061 -0.434 NA	-0.056 NA NA	0.000	0.000	-0.500	0.00	0.00	0.00
CASE 5	CFD IFM DATA	0.352 -0.072 NA	-0.495 -0.065 NA	-0.981 -0.329 NA	-0.816 -0.344 NA	-0.046 NA NA	0.000	0.000	-1.000	0.00	0.00	0.00
CASE 6	CFD IFM DATA	0.066 -0.060 NA	-0.147 -0.015 NA	-0.337 -0.165 NA	-0.256 -0.135 NA	-0.045 NA NA	0.000	0.000	-4.000	0.00	0.00	0.00
CASE 7	CFD IFM DATA	0.706 0.363 0.889	1.346 0.951 1.250	-1.157 -0.566 -1.243	0.718 0.352 0.394	-0.035 NA 0.007	0.498	-0.186	-2.484	-12.37°	2.76°	-6.50°

the segment centerline (obtained from the CFD solution of the isolated wing/pylon calculation) to predict the force and moment coefficients, as described in section 4.1. The angles and influence coefficients used are shown in Fig. 5.7. The first and last of the ANCN and BNCLM coefficients are the largest; a result which stresses the importance of the store's nose and tail. The ANCN influence coefficients for the IFM are all positive and therefore indicate that the forces on the segments will be in the direction of the upwash and sidewash. The BNCLM coefficients have positive and negative values, positive near the nose and negative near the tail. This coefficient distribution indicates that positive angles creating a positive moment on the nose will be counteracted by those positive angles creating a negative moment on the tail. The sum of the coefficients near the nose is very similar to the sum of those at the tail, thus, according to the IFM, this store should be relatively stable. Given uniform flow angles, the moments created by the nose will be negated by the moments on the tail.

The agreement between the CFD and the IFM force and moment coefficients in Table 5.1 is surprisingly poor in all cases. It was expected that, starting at 1 diameter below the carriage position, the IFM would produce force coefficients that matched the CFD calculations, but this was not the case. As can be seen in Fig. 5.7, most of the upwash angles are negative, thus the normal force predicted by the IFM is downward. However, the data and CFD predictions show an upward normal force resulting from the low pressure between the wing and store (an effect which the IFM has no way of forecasting). This low pressure area can be seen in the pressure coefficient contours shown in Fig. 5.8. The double contour lines arise from the overlapping grid information. This figure also illustrates why mutual interference is so pronounced. At the pylon station, the length of the store is almost as long as the local wing chord and its diameter is larger than the wing thickness. The IFM side force, pitching moment, and yawing moment are grossly underpredicted in most cases although the signs are correct. The mutual interference is creating pressure effects for which the IFM cannot account. A comparison of the pressure coefficient contours for the underside of the isolated wing/pylon and the wing/pylon with the store one and four diameters

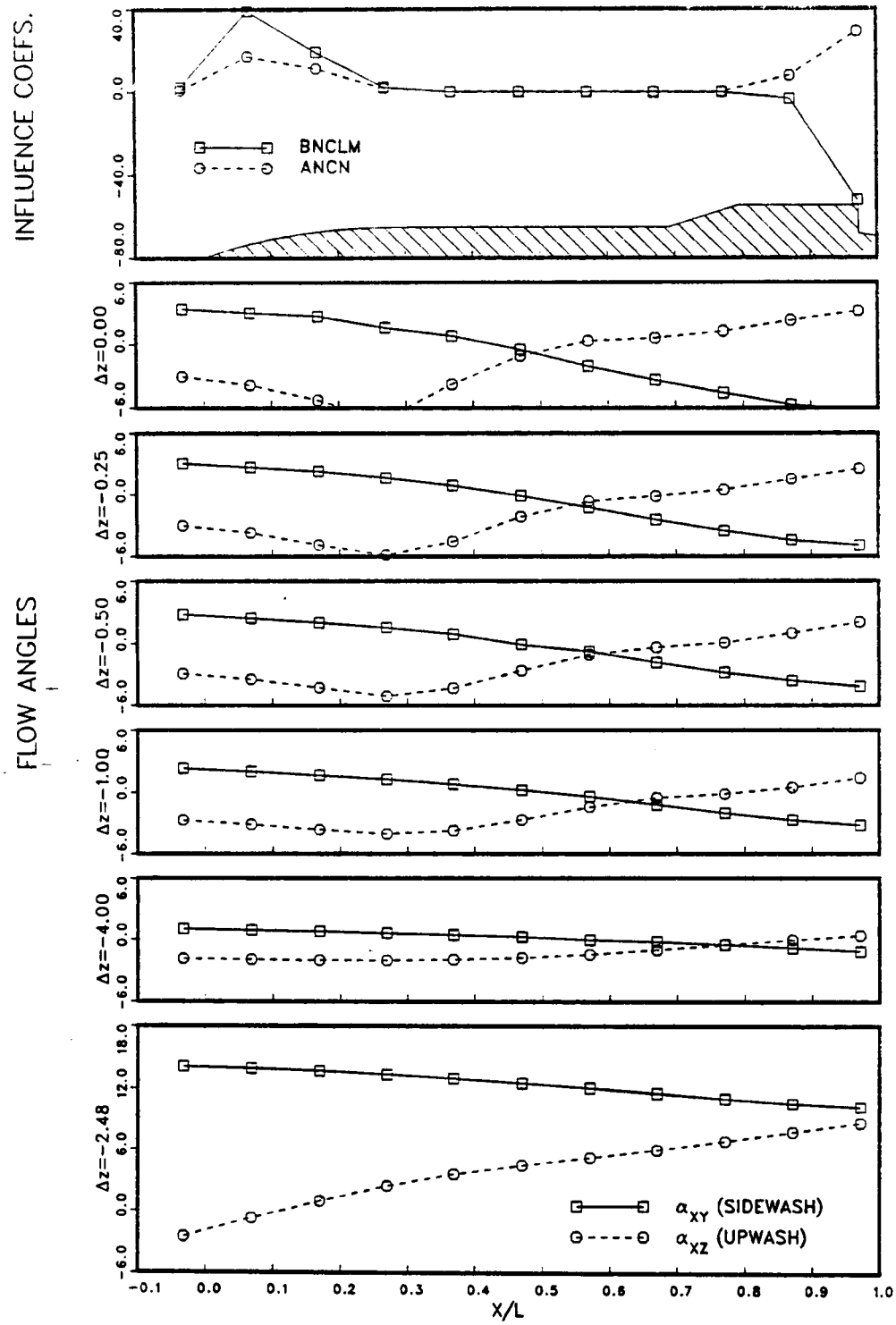

Figure 5.7: IFM influence coefficients and associated flow angles

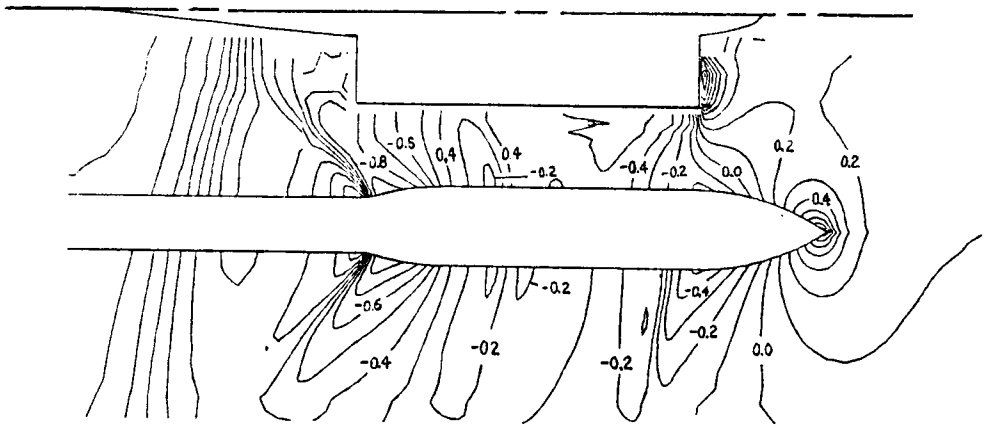

a. Store Δz= -1.0 DIA

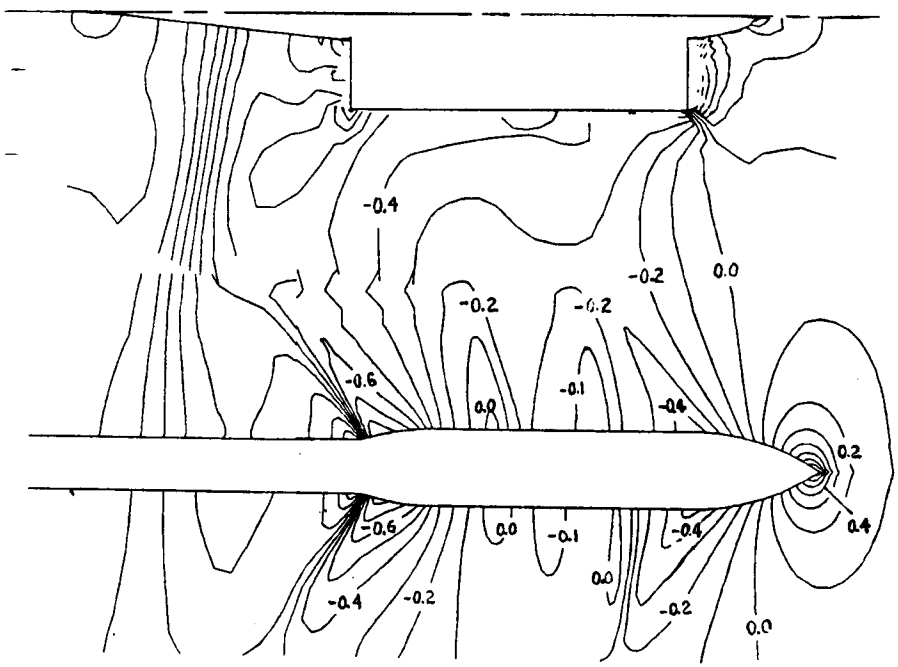

b. Store Δz= -4.0 DIA

Figure 5.8: Pressure coefficient contours along store symmetry plane

away is presented in Fig. 5.9. The effects of the mutual interference can be seen in this figure also. Further calculations are required to determine precisely where the mutual interference ends. However, if the load coefficients predicted by the CFD calculations and IFM are extrapolated, the curves intersect somewhere between five and six store diameters away from the carriage position.

Because the IFM and CFD predictions differed so drastically, it was desirable to seek additional confirmation of the CFD predictions. Therefore, the IFM and CFD loads were compared to measured loads at a trajectory position determined in the wind tunnel CTS test. To match the position, the store c.g. was translated 0.498 store diameters downstream, 2.484 diameters downward, and 0.186 diameters toward the wing symmetry plane from the carriage position. The store was then yawed -12.37 degrees about the store's z axis, then pitched 2.76 degrees about its y axis, and then rolled -6.50 degrees about its x axis (see Fig. 5.10). It should be noted that the -12.37 degree yaw angle rotated the downstream end of the sting inward past the vertical symmetry plane, but the reflection boundary condition used by XMER3D was not modified. It was felt that the error introduced would be small since the intersection occurred approximately three store lengths downstream of the base of the store. Also, the above Euler angles included the adjustments for translational velocity effects on the store as discussed in Section 4.1. Pitch and yaw damping were accounted for in the calculation of the moments by using the damping derivatives that were used in the wind tunnel test. A damping factor is calculated by multiplying rate damping derivatives (usually found empirically) by the rotation rates determined in the test. This factor is then simply added to the calculated moments. The resulting CFD pressure distributions and CFD and IFM load predictions for the calculation are shown in Fig. 5.11 and Table 5.1, respectively. The measured and calculated pressure distributions compare very well on the store body, but the pressure on the fins was not predicted very well by the calculations. At the $\phi = 45$ and 225 degree fin locations, a small separation region on the lee side that appears in the data does not appear in the calculations. The fin pressure data on the lee side of the store ($\phi = 225$ and 315 degrees) do not match very well on either side of the fins. The pressure error on the fins resulted in discrepancies

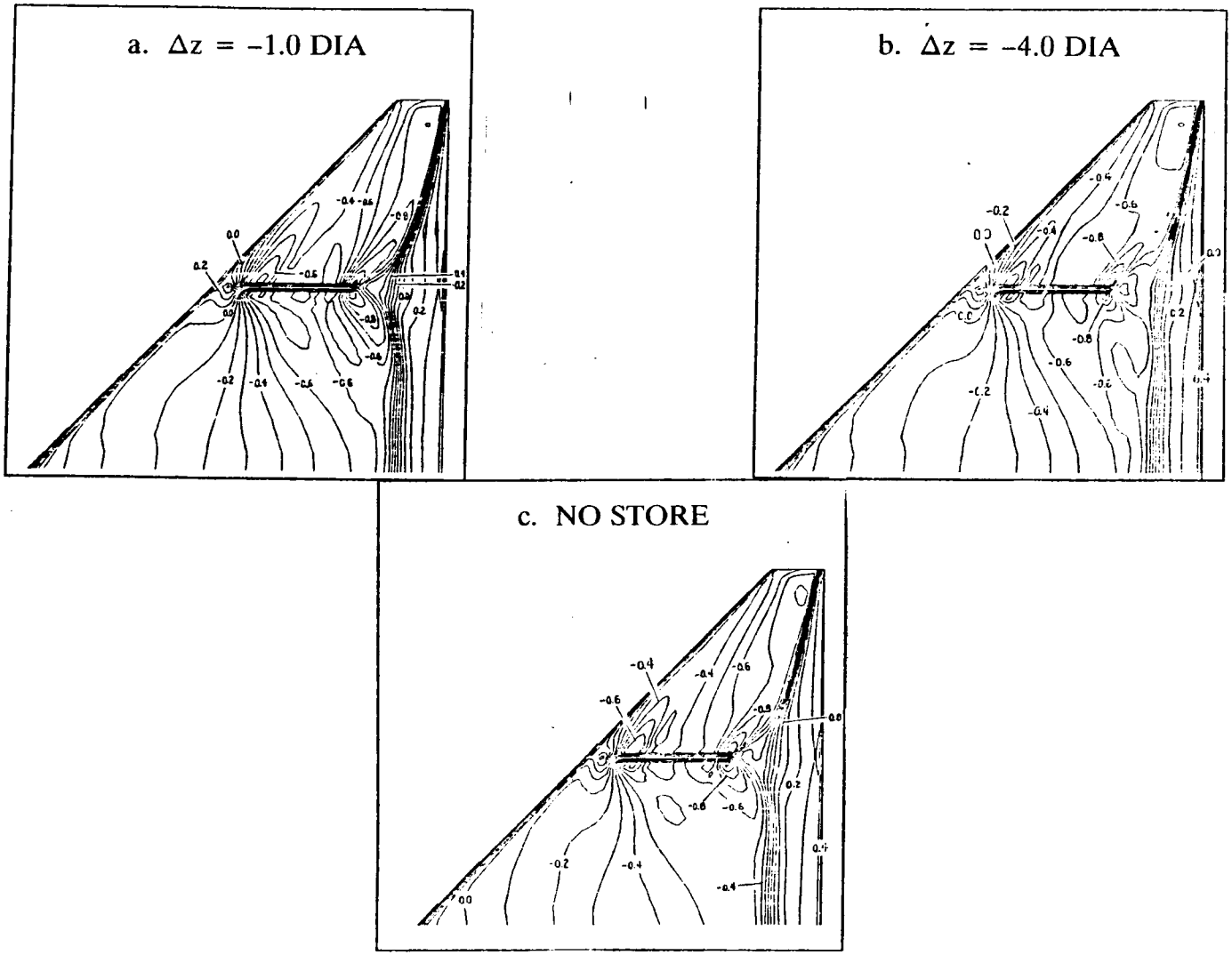

Figure 5.9: Wing lower surface pressure coefficient contours

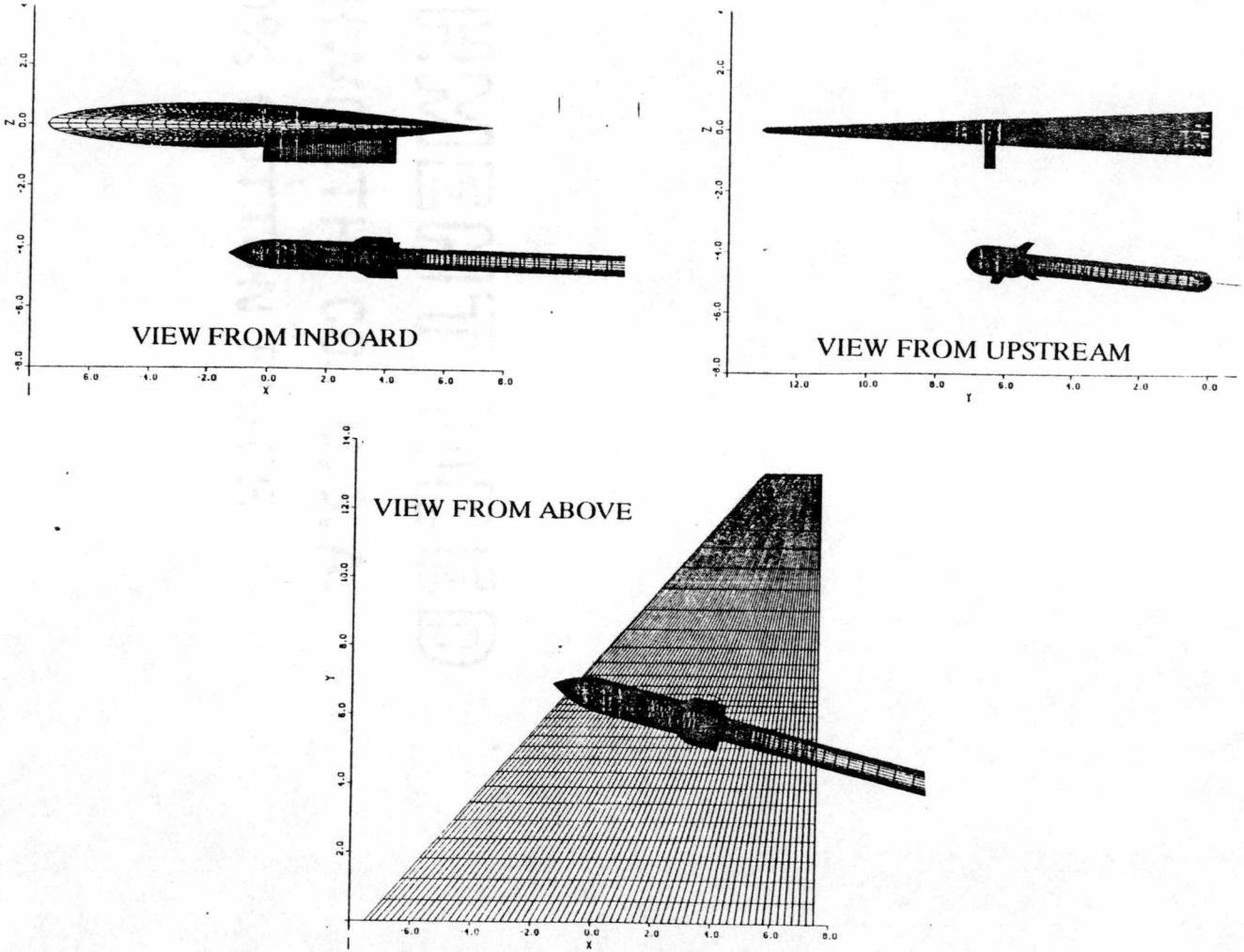

Figure 5.10: Store in trajectory position

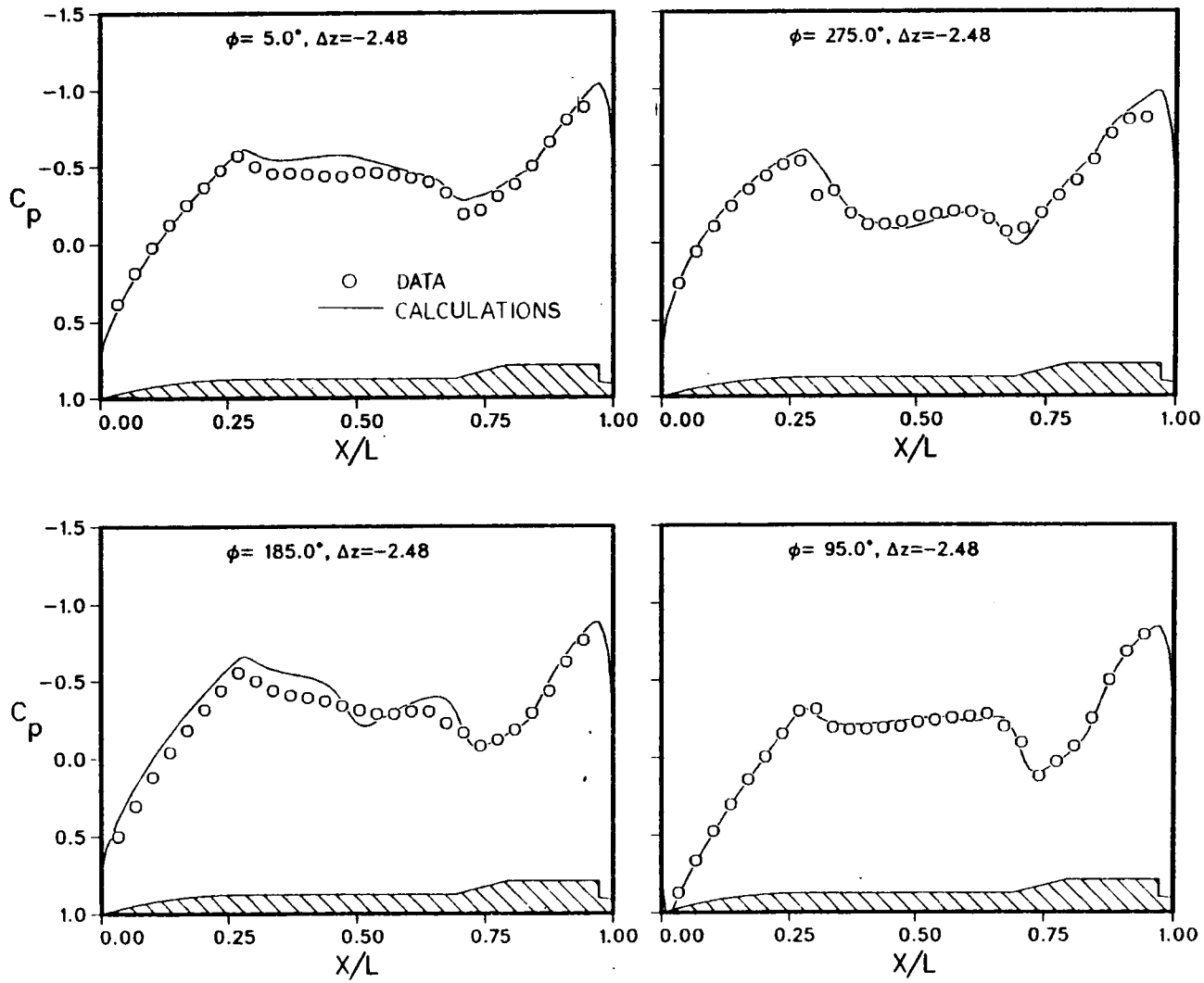

Figure 5.11: Pressure coefficient distribution at the trajectory position
a. Body distribution

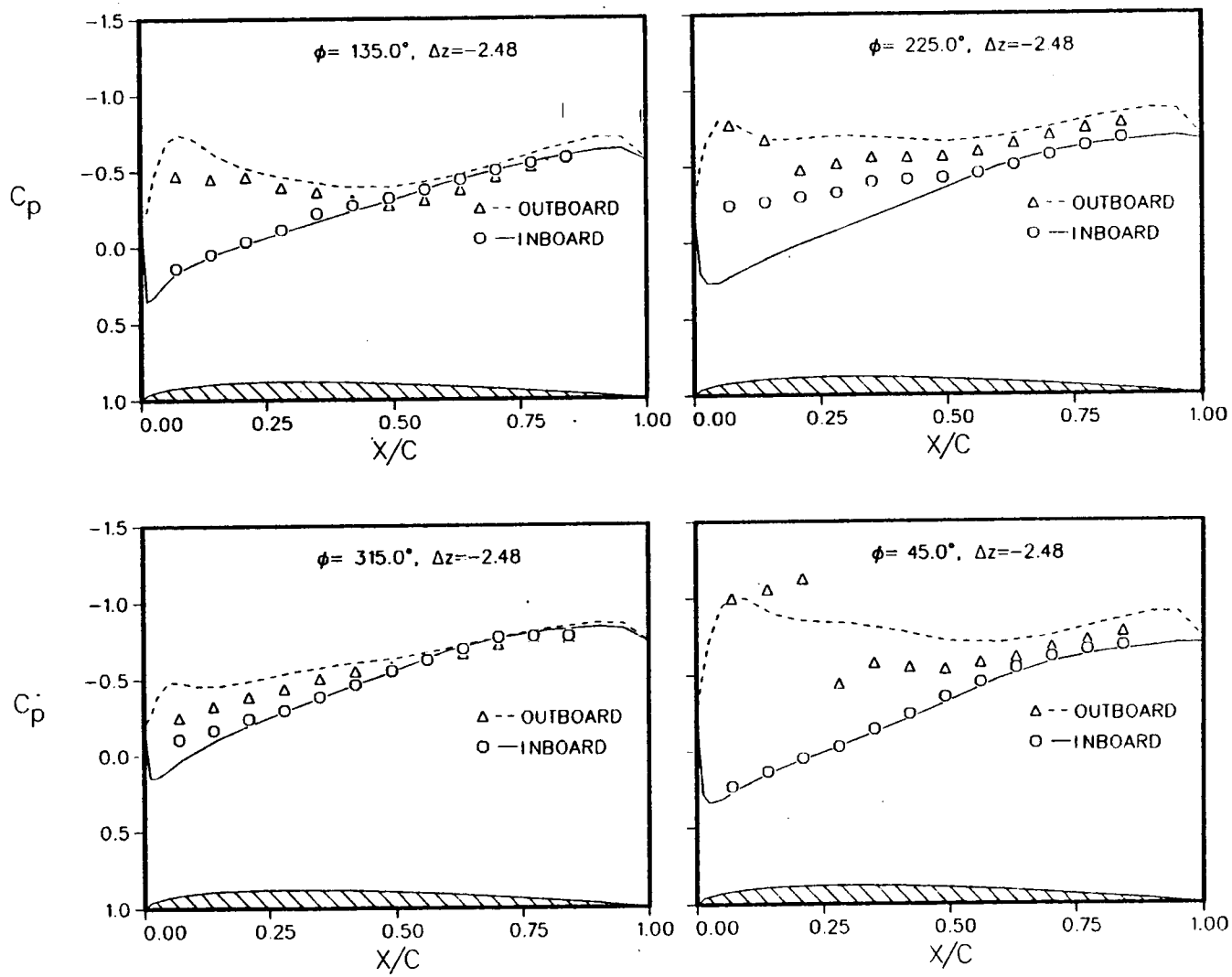

Figure 5.11: Concluded
b. Fin distributions

with the data, particularly in the normal force and yawing moment predicted by the calculations. The IFM loads show very poor agreement with both the calculated and measured data. Little can be said about the IFM predictions. Either the influence coefficients or the calculated flow angles are incorrect, and it is strongly suspected that the problem lies with the influence coefficients. Strictly speaking, the IFM load predictions are valid only for flow angles smaller than the flow angle used in the store calibration program which determes $ANCN_i$ and $BNCLM_i$. A five degree flow was used to calibrate this store; yet for case 7, some of the flow angles were over twice that amount, as can be seen in Fig. 5.7. For the above reasons, it is more believable that the CFD loads for cases 2-6 are more nearly correct than are the IFM-predicted loads.

After the differences in the loads were found, a question arose as to how much these differences affect the store's trajectory. To address this question, a six degree-of-freedom computer program was used to predict the motion of the store over a 10 millisecond time step. The starting position used was the same position used in case 7. The rotational and translational motion of the store predicted by the wind tunnel test were included in the calculations. The results are shown in the table below, where the Δ refers to the change between the previous and current location.

	Δ x	Δ y	Δ z	Δ Yaw	Δ Pitch	ΔRoll
Test Loads	0.04	-0.02	-0.09	-0.36°	-0.50°	-0.43°
CFD Loads	0.04	-0.02	-0.09	-0.35°	-0.50°	-0.43°
IFM Loads	0.04	-0.02	-0.09	-0.37°	-0.48°	NA

Of course, very little information concerning the entire trajectory can be deduced from a single point. However, at this point, the difference between the motion predicted using the CFD and tunnel-measured loads and the difference between the IFM and tunnel-measured motion are both less than the measurement uncertainties stated in the test documentation. For this store at

this point in its trajectory, yaw, roll, and the x and y coordinates of the c.g. are a result of the aerodynamic loads, but the primary contributors to the pitch and z coordinate of the c.g. are the full-scale weight of the store (2,000 lbs) and the normal force and pitching moment imparted by the ejectors that expel the store from the pylon (12,000 lbs and 8952 ft-lbs, respectively). However, this overriding of the pitch-plane aerodynamic loads by the loads at release cannot be said to be true in general. The weight and ejector forces of other stores may be much closer to the aerodynamic forces, the control surfaces may be more effective, the ejector forces may not be limited to the pitch-plane, and at some point in the trajectory, the accelerations imparted by the ejectors may be reduced to a level at which the aerodynamic loads become paramount.

Another objective of this study was to investigate the carriage-load correction to the IFM (see section 4.2). The fact that the IFM results agree so poorly with the CFD calculations make this difficult, but not impossible. If each IFM-predicted load coefficient for the cases between carriage position and one store diameter down is shifted upward by a constant amount so that the coefficients at one diameter match the CFD coefficients, the correction can be applied and perhaps give an estimate as to the accuracy of the correction. The resulting curves and the corrected curves are shown in Fig. 5.12a. As can be seen in the Figure, the corrected coefficients and the CFD calculations agree very well. This shift operation can also be performed for the cases between the carriage position and 4 diameters downward. Figure 5.12b shows the resulting curves for this case. The agreement between the corrected coefficients and the CFD coefficients has degraded slightly, but is still reasonable.

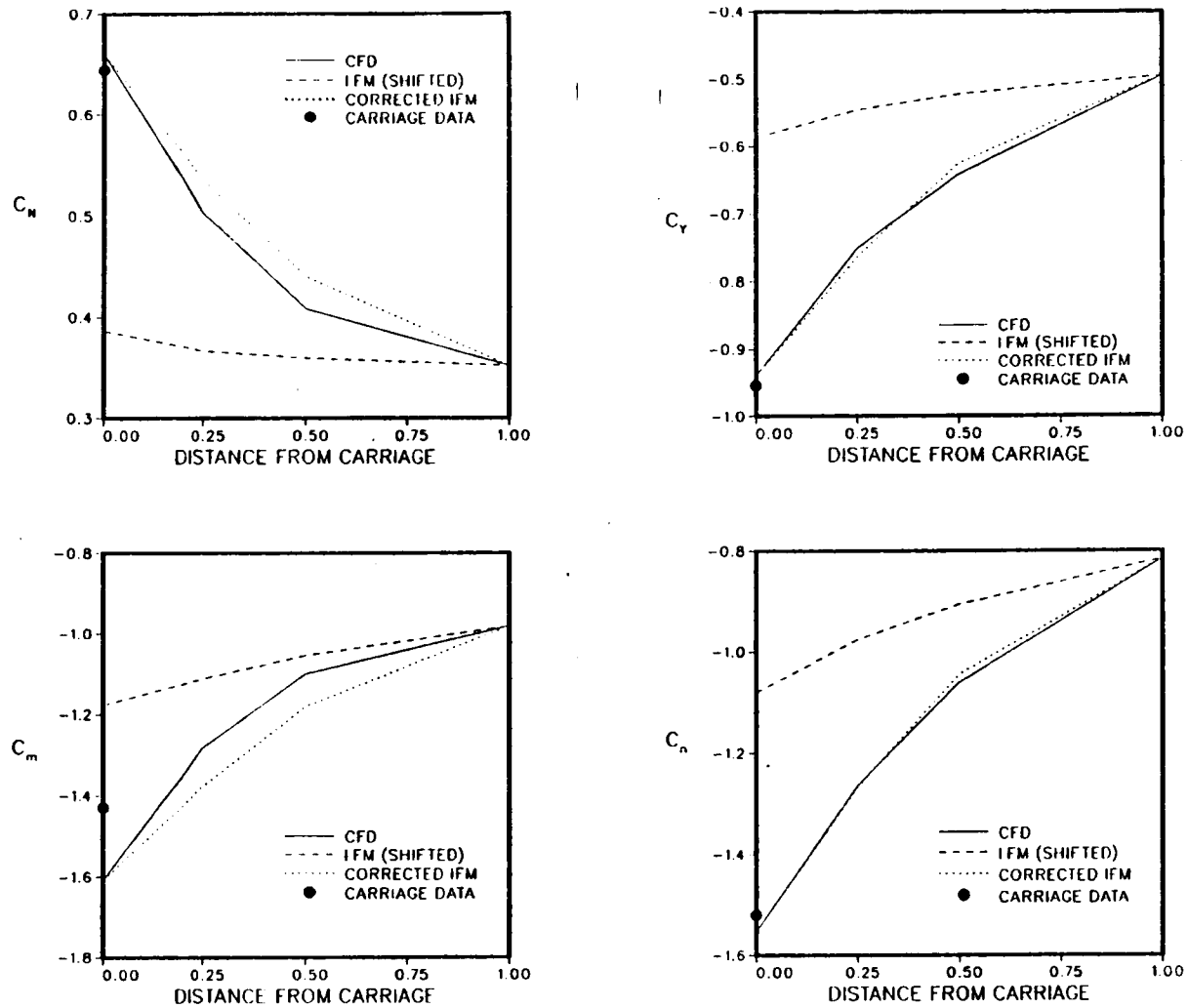

Figure 5.12: IFM carriage load corrections
a. Mutual interference ending at 1.0 DIA

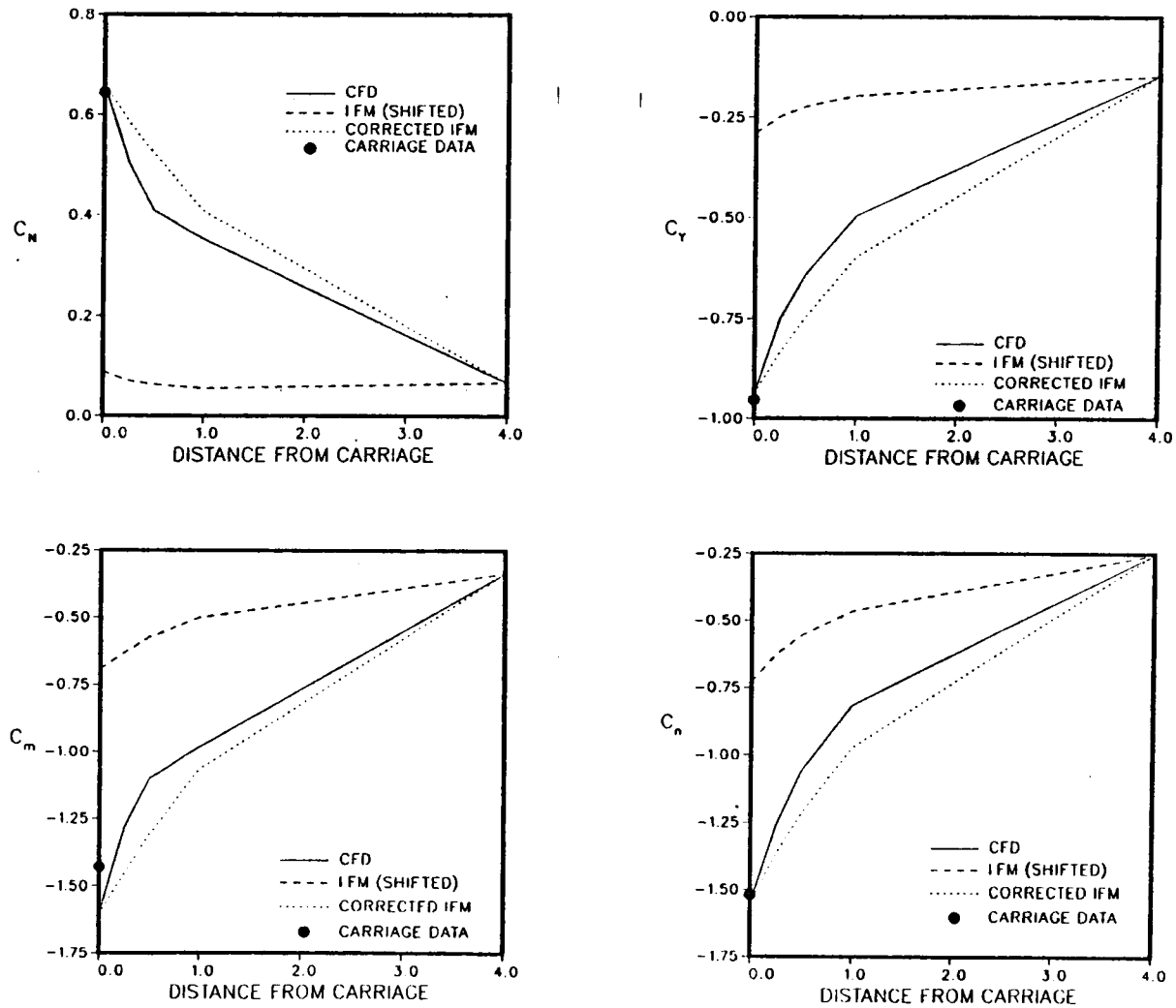

Figure 5.12: Concluded

b. Mutual interference ending at 4.0 DIA

Chapter 6

CONCLUSIONS

The results of these calculations lead to the following conclusions:

- The computational method that should be used to predict the store trajectory will be extremely dependent on the physical properties of the store, the method of release, and the location of the store in the overall trajectory. Massive stores released with large ejector forces are affected little by local aerodynamics in the early stages of the trajectory; therefore, using inviscid calculations, simplifications to the geometry, or a relatively coarse grid might result in acceptable answers. Stores with small mass, or stores with large control surfaces, or massive stores well away from the parent craft will require much more care since the aerodynamic loads will be the primary contributors to the trajectory. Wind tunnel tests or viscous calculations might be warranted. In this study, the motion of the store from the chosen trajectory position was very insensitive to the aerodynamic loads because of the store's large mass and the large ejector forces used to jettison the store. The motions resulting from the IFM and CFD loads, despite the differences in the load predictions, both matched the motion resulting from the measured loads reasonably well for this configuration.

- Geometric fidelity, even on the fins, can be important. (In this study, approximately half of the total aerodynamic forces was attributable to the fins.) Therefore, once the aerodynamic loads become paramount, geometric simplifications might significantly alter the total loads,

and thus alter the trajectory of the store.

- The inviscid CFD predictions for the store pressure distributions and force and moment coefficients agreed very well with test data at carriage and fairly well with data at the trajectory position.

- The mutual interference correction to the loads predicted by the IFM gives reasonable approximations to the CFD predicted loads, providing the distance over which the mutual interference decays to insignificance is known. The basic IFM without the correction cannot reliably predict the store loads if mutual interference effects are present.

- The assumption that mutual interference is no longer significant at one store diameter away from the carriage position is not valid for the store in this study. Computational results indicate that a distance of five to six store diameters is necessary before mutual interference effects disappear.

The above conclusions lead to suggestions for possible future study, such as

- A study might be initiated to obtain appropriate size parameters to use as a guideline in determining the distance necessary for the store to be moved for mutual interference to cease.

- Calculations matching a portion of a CTS test might be performed to prove the ability of CFD to predict a trajectory. Because of the CPU time required, a solution at each of the approximately 100 trajectory locations used in a tunnel test is not recommended.

BIBLIOGRAPHY

Bibliography

[1] Keen, K.S. "New Approaches to Computational Aircraft/Store Weapons Integration." AIAA Paper No. 90-0274, January 1990.

[2] Nadir, S. and Wedan, B.W. "The Northrop-NEAR Subsonic Store Separation Prediction Method." Paper presented at the 6th Biennial Aircraft/Stores Compatibility Symposium, October 1982.

[3] Fox, J.H. and Allee, E.G. "Experimental/Computational Study of a Transonic Aircraft with Stores." AIAA Paper No. 89-1232, June, 1989.

[4] Donegan, T.L. and Fox, J.H. "Analysis of Store Trajectories from Tactical Fighter Aircraft." AIAA-91-0183, January 1991.

[5] *Test Facilities Handbook* (Eleventh Edition). "Propulsion Wind Tunnel Facility." Vol. 4, Arnold Engineering Development Center, June 1979.

[6] Carman, J.B., Hill, D.W., and Christopher, J.P. "Store Separation Techniques at the Arnold Engineering Development Center." AEDC-TR-79-1, Vol. II, June 1980.

[7] Benek, J.A., Steger, J.L., Dougherty, F.C., Buning, P.G. "Chimera: A Grid Embedding Technique." AEDC-TR-85-64, April 1986.

[8] Dietz, W.E. and Suhs, N.E. "PEGSUS 3.0 User's Manual." AEDC-TR-89-7, August 1989.

[9] Dietz, W.E. and Evans, S.B. "Interactive EAGLE: An Interactive Surface Mesh and Three-Dimensional Grid Generation System." AEDC-TR-90-25, December 1990.

[10] Thompson, J.F. "A Composite Grid Generation Code for General 3D Regions- The EAGLE Code." AIAA Journal, Vol. 26, No. 3, March 1988, pp. 271-272.

[11] Pulliam, T.H. and Steger, J.L., "Implicit Finite-Difference Simulations of Three Dimensional Compressible Flow." AIAA Journal, Vol. 18, No. 2, February 1980, pp. 156-169.

[12] Beam, R. and Warming, R.F. "An Implicit Finite Difference Algorithm for Hyperbolic Systems in Conservation Law Form." Journal of Computational Physics, Vol. 22, September 1976, pp. 87-110.

[13] Anderson, D.A., Tannehill, J.C. and Pletcher, R.H., "*Computational Fluid Mechanics and Heat Transfer,*" Hemisphere Publishing Corporation, New York, 1984 (First Edition).

[14] Jameson, A. and Baker, T.J. "Solution of the Euler Equations for Complex Configurations." AIAA 83-1929, July 1983.

[15] Kraft, E.M., Ritter, A., and Laster, M.L. "Advances at AEDC in Treating Transonic Wind Tunnel Wall Interference." ICAS-86-1.6.1, ICAS Proceedings, 15th Congress of the International Council of the Aeronautical Sciences, London/UK, Vol. 2, pp.748-769, September 1986.

VITA

Jefferson Keith Jordan was born in Somerville, Tennessee on November 1, 1961. He attended elementary schools in Hardeman County, Tennessee and graduated from Middleton High School (also in Hardeman County) in 1980. The following fall semester, he enrolled at Mississippi State University, and in May of 1985 he received a Bachelor of Science degree in Aerospace Engineering. In August of 1985, he entered the University of Tennessee and in December, 1991 received a Master of Science Degree in Aerospace Engineering.

Mr. Jordan is currently employed as a Research Engineer for Calspan Corporation at the Arnold Engineering Development Center, Arnold Air Force Base, Tennessee, and lives in nearby Tullahoma with his family.